Cell

Inhibition of SRGAP2 Function by Its Human-Specific Paralogs Induces Neoteny during Spine Maturation

Cécile Charrier,[1,7] Kaumudi Joshi,[1,7] Jaeda Coutinho-Budd,[2] Ji-Eun Kim,[3] Nelle Lambert,[4,5] Jacqueline de Marchena,[2,8] Wei-Lin Jin,[6] Pierre Vanderhaeghen,[4] Anirvan Ghosh,[3] Takayuki Sassa,[1,9] and Franck Polleux[1,*]

[1]Department of Cell Biology, Dorris Neuroscience Center, The Scripps Research Institute, La Jolla, CA 92037, USA
[2]Neuroscience Center, University of North Carolina at Chapel Hill, Chapel Hill, NC 27599, USA
[3]Neurobiology Section, University of California, San Diego, La Jolla, CA 92093, USA
[4]IRIBHM, Université Libre de Bruxelles, Brussels B-1070, Belgium
[5]Department of Medical Genetics, Hôpital Erasme-ULB, Brussels B-1070, Belgium
[6]School of Life Sciences and Biotechnology, Shanghai Jiao Tong University, Shanghai 200240, China
[7]These authors contributed equally to this work
[8]Present address: National Institute of Environmental Health Science, 111 T.W. Alexander Drive, Research Triangle Park, NC 27709, USA
[9]Present address: Faculty of Pharmaceutical Sciences, Hokkaido University, Sapporo 060-0812, Japan
*Correspondence: polleux@scripps.edu
DOI 10.1016/j.cell.2012.03.034

SUMMARY

Structural genomic variations represent a major driving force of evolution, and a burst of large segmental gene duplications occurred in the human lineage during its separation from nonhuman primates. *SRGAP2*, a gene recently implicated in neocortical development, has undergone two human-specific duplications. Here, we find that both duplications (*SRGAP2B* and *SRGAP2C*) are partial and encode a truncated F-BAR domain. SRGAP2C is expressed in the developing and adult human brain and dimerizes with ancestral SRGAP2 to inhibit its function. In the mouse neocortex, SRGAP2 promotes spine maturation and limits spine density. Expression of SRGAP2C phenocopies SRGAP2 deficiency. It underlies sustained radial migration and leads to the emergence of human-specific features, including neoteny during spine maturation and increased density of longer spines. These results suggest that inhibition of SRGAP2 function by its human-specific paralogs has contributed to the evolution of the human neocortex and plays an important role during human brain development.

INTRODUCTION

In recent years, many potential genetic mechanisms have been proposed to participate in human brain speciation. These include changes in transcriptional regulation (Enard et al., 2002; Konopka et al., 2009), accelerated evolution of small noncoding RNAs (Pollard et al., 2006), changes in the activity and/or region-specificity of enhancer elements (McLean et al., 2011; Prabhakar et al., 2006, 2008) or changes in patterns of alternative splicing (Calarco et al., 2007). So far, very few studies have assessed the functional consequences of these changes. Another important mechanism is genomic duplication, which generates copies of genetic material that serve as substrates for molecular evolution (Hurles, 2004; Ohno, 1970). In fact, recent lines of evidence have revealed that a burst of large segmental gene duplications occurred in the human lineage during its separation from nonhuman primates approximately 6 million years ago (Bailey et al., 2002; Fortna et al., 2004). Several of the genes contained in these duplications are expressed in the developing brain. This has led to the hypothesis that these evolutionarily recent gene duplications might have participated in the emergence of human-specific features of brain development and function (Bailey and Eichler, 2006; Sikela, 2006; Stankiewicz and Lupski, 2010; Varki et al., 2008). However, this hypothesis has never been tested experimentally. The principal obstacles have been that the function of the ancestral genes is often unknown and that the duplications are poorly assembled in the current human genome because of their high degree of conservation with the ancestral gene.

In this study, we focused on SLIT-ROBO Rho-GTPase-activating protein 2 (*SRGAP2*), a gene highly expressed during brain development (Bacon et al., 2009; Guerrier et al., 2009). The protein SRGAP2 is composed of three functional domains (Guerrier et al., 2009): an N-terminal F-BAR (Bin, Amphiphysin, Rvs) domain (Itoh et al., 2005) involved in membrane deformation, a central Rho GTPase-Activating Protein (Rho-GAP) domain that specifically stimulates the GTPase activity of Rac1, and a C-terminal tail containing an SH3 domain. We previously demonstrated that SRGAP2 controls cortical neuron migration (Guerrier et al., 2009). Recent analysis of large segmental duplications has revealed that *SRGAP2* has two main duplicates in the *Homo neanderthalensis* and *Homo sapiens* genomes, but not in the genome of our closest living

relatives, the chimpanzee, orangutan and gorilla (Sudmant et al., 2010). In this study, we mapped the location and genomic structure of the human-specific *SRGAP2* paralogs (see also accompanying article by Dennis et al. [2012] in this issue of *Cell*). We provide evidence that they are expressed in human neurons and encode a truncated F-BAR domain that interacts with ancestral SRGAP2 to inhibit its function. We used in vitro and in vivo approaches to determine the function of SRGAP2 and its human paralogs in the neocortex region of the brain, the evolution of which is thought to underlie the emergence of human cognitive abilities. Our results uncover a new function for ancestral SRGAP2 in promoting dendritic spine maturation and indicate that expression of a human-specific paralog of SRGAP2 in mouse pyramidal neurons extends the phase of spine development and leads to an increased density of longer spines in vivo, a feature characterizing pyramidal neurons in the human neocortex (Benavides-Piccione et al., 2002; Elston et al., 2001).

RESULTS

Genomic Organization of *SRGAP2* Paralogs

The gene *SRGAP2* was identified by using array comparative genomic hybridization (aCGH) as having undergone human-specific duplication, resulting in extra copies in the *H. sapiens* genome, but not in the genomes of four nonhuman primates (Fortna et al., 2004). However, the number and locations of these human-specific copies were unknown. Using the Blast-Like Alignment Tool (BLAT), we searched the GRCh36/hg18 reference genome (available human genome assembly in 2006 at the start of the project) with the cDNA of human *SRGAP2* (GenBank BC132874.1). We located the ancestral *SRGAP2* gene at chromosome 1q32.1 (*SRGAP2A*) and two duplicates at 1q21.1 and 1p12 (hereafter referred to as *SRGAP2B* and *SRGAP2C*, respectively) that showed more than 99% similarity to the query sequence (Figures S1A and 1B available online). The observation that there are two duplicates of *SRGAP2* in the human genome was recently confirmed and validated by analysis of copy number variation in whole-genome shotgun sequencing data (Sudmant et al., 2010). Even in the most recent reference assembly (GRCh37/hg19), the ancestral *SRGAP2A* gene is classified as misassembled, and *SRGAP2B* and *SRGAP2C* lie in recently duplicated regions of the genome that are incompletely assembled and present large contig gaps. In order to determine the approximate genomic organization of these three paralogs, we retrieved human bacterial artificial chromosome (BAC) clones mapping to these three loci. To fill in the gaps in the assembled sequence, we performed BLAST searches against the end sequences database by using genome sequences flanking the gaps as inputs. The exon organization of the human BACs was determined by dot blot hybridization with several probes covering different portions of the entire extent of *SRGAP2* cDNA (data not shown). In addition, exons in each BAC clone were sequenced from the human BAC DNA either directly before or following amplification to reveal the organization of the three *SRGAP2* paralogs (data not shown, Figure S1C). The full sequencing and assembly of the three genomic loci and their recent evolution is the focus of the accompanying paper by Dennis et al. (2012). Both analyses revealed that *SRGAP2A* contains 22 exons and encodes a protein with 1,071 amino acids (aa), which is 98% identical to its mouse ortholog SRGAP2, whereas *SRGAP2B* and *SRGAP2C* have a 3′ breakpoint located in intron 9 of the ancestral copy and are predicted to express a protein containing 459 aa. The first 452 aa correspond to the first 452 aa of the F-BAR domain of SRGAP2A (aa1-501; Guerrier et al., 2009). Because intron 9 of *SRGAP2A* becomes 3′ untranslated region (3′ untranslated region [UTR]) in *SRGAP2B* and *SRGAP2C*, both use an alternate stop codon located in intron 9, which adds 7 aa (VRECYGF; Figure 1A). We identified two potential polyadenylation sites in the 3′ UTRs of *SRGAP2B* and *SRGAP2C* based on the clustering of expressed sequence tags (EST) from the database of Expressed Sequence Tags (dbEST). The two 3′ UTRs are ~1.4 kb or 5 kb long. Taken together, our results indicate that both paralogs encode a truncated F-BAR domain that lacks the last C-terminal 49 aa.

Expression of *SRGAP2* Paralogs

We isolated one cDNA clone from a human library (GenBank BC112927.1) originating from *SRGAP2C* that is almost identical in sequence to the first 9 exons of the ancestral *SRGAP2A*, except for five nonsynonymous base pair mutations (out of 1,356 base pairs) mutating five arginine (5R) residues (Figure 1A). As shown in the accompanying paper by Dennis et al. (2012), *SRGAP2B* and *SRGAP2C* are identical apart from a few base pair mutations, and both lack the last 49 aa of the F-BAR domain. In order to determine the expression of these human-specific paralogs in the brain, we took advantage of the fact that intron 9 becomes 3′ UTR in *SRGAP2B* and *SRGAP2C* to perform in situ hybridization (ISH) on cryostat sections from human fetal cortex (gestational week [GW] 11). *SRGAP2B* and *SRGAP2C* were therefore detected using an intron 9 probe that does not recognize processed mRNA encoding ancestral *SRGAP2A*, whereas *SRGAP2A* was detected using an exon 22 probe that conversely does not recognize *SRGAP2B* or *SRGAP2C* (Figures 1A and 1B and data not shown). This analysis revealed a striking similarity in the pattern of expression of the paralogs in the germinal layers (ventricular zone [VZ] and subventricular zone [SVZ]), in which neural progenitors divide to produce postmitotic neurons. We also detected significant expression in the cortical plate (Figure 1B), in which neurons end their migration and undergo terminal differentiation and synapse formation. To refine this gene expression analysis, we took advantage of the possibility to differentiate human embryonic stem cells (hESCs) into relatively pure populations of forebrain excitatory pyramidal neurons (Kim et al., 2011). Total RNA was harvested from hESCs at different time points during their directed differentiation in vitro (Kim et al., 2011), allowing us to perform a temporal analysis using reverse-transcriptase PCR (RT-PCR) primers (Figure 1C and Table S1), amplifying *SRGAP2A* (exon 10-11 junction) or *SRGAP2B* and *SRGAP2C* (intron 9) transcripts. Both ancestral and human-specific paralogs of *SRGAP2* were detected at low levels in undifferentiated hESCs that express *OCT4* (lane 1 in Figure 1C). Their expression increased in a mixture of neural progenitor cells (*PAX6*+) and immature neurons (*TUJ1*) (3 weeks in culture [wic], Kim et al., 2011; lane 2 in Figure 1C) as well as in more mature, synaptically active, *PSD95*-expressing

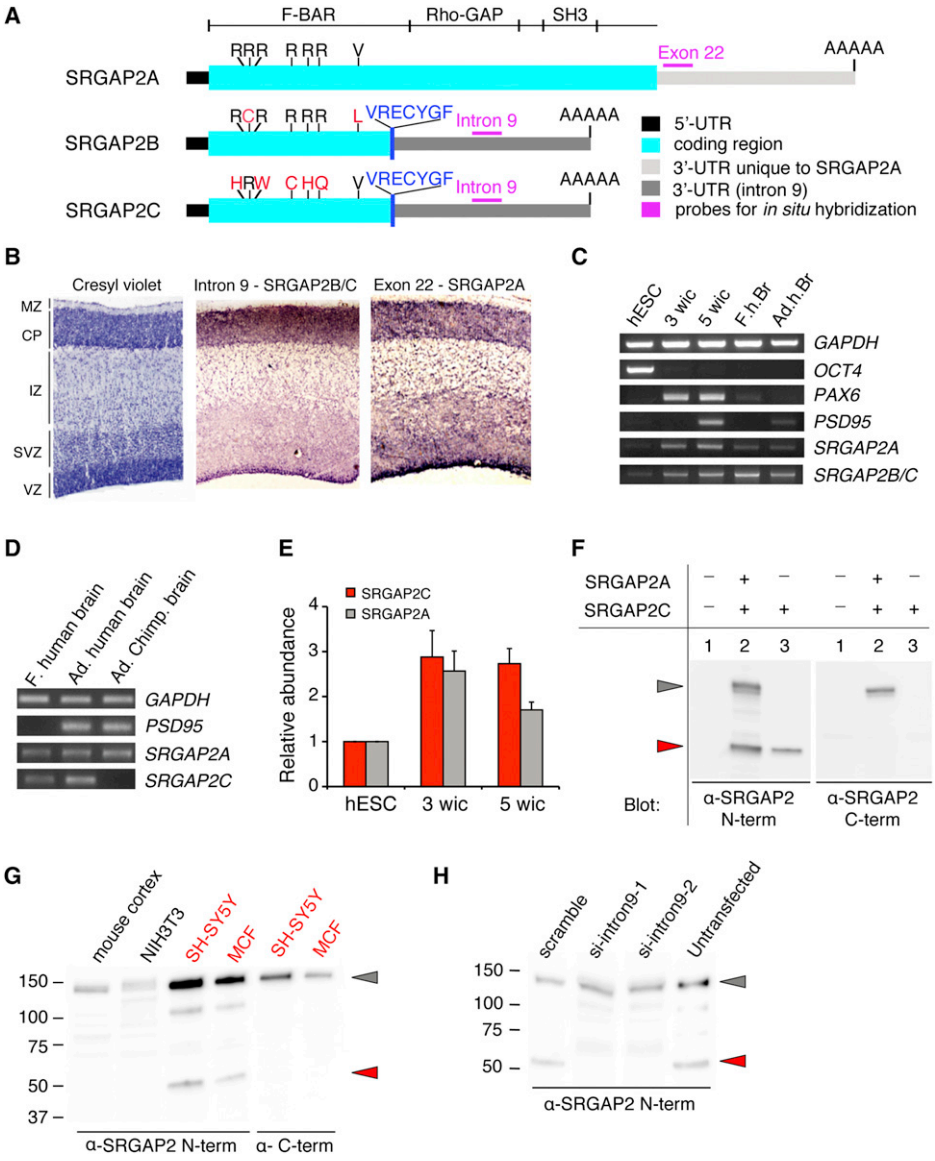

Figure 1. SRGAP2 and Its Human-Specific Paralogs Are Expressed in Human Neurons

(A) Schematic representation of transcripts of the three paralogs of *SRGAP2*. *SRGAP2B* and *SRGAP2C* encode a truncated F-BAR domain with nonsynonymous mutations marked in red. VRECYGF denotes C-terminal aa residues translated from intron 9 that are unique to *SRGAP2B* and *SRGAP2C*.

(B) RNA in situ hybridization on developing human cortex at GW 11 using probes specific for *SRGAP2B* and *SRGAP2C* (intron 9) and *SRGAP2A* (exon 22). Cresyl violet marks the cortical layers: VZ (ventricular zone), SVZ (subventricular zone), IZ (intermediate zone), CP (cortical plate), and MZ (marginal zone).

(C) RT-PCR showing that *SRGAP2A*, *SRGAP2B*, and *SRGAP2C* are expressed in OCT4+ hESCs, neurons derived from hESCs following 3 wic (PAX6+, PSD95-) or 5 wic (PSD95+), as well as fetal human brain (F.h.br) and adult human brain (Ad.h.Br).

(D) RT-PCR performed on RNA from fetal (f.) human brain, adult (Ad.) human brain and adult chimpanzee (Ad. Chimp) brain samples. *SRGAP2A* primers detect the ancestral copy in human and chimp samples. *SRGAP2C* primers show an amplification band specifically in the human samples, indicating stringency of primer hybridization only to the *SRGAP2C* variant.

(E) qRT-PCR showing relative abundance of *SRGAP2C* and *SRGAP2A* in samples corresponding to lanes 1, 2, and 3 in (C) normalized to levels of GAPDH (mean ±SD; standard deviation from two technical replicates).

(F) Full-length SRGAP2A detected by western blotting with anti (α)-SRGAP2 N-terminal or anti-SRGAP2 C-terminal when transfected in HEK293T cells (grey arrowhead). The anti-SRGAP2 N-terminal, but not the anti-SRGAP2 C-terminal, can detect SRGAP2C (red arrowhead).

(G) A translation product corresponding to the human-specific paralogs SRGAP2B or SRGAP2C in size (50 kDa; red arrowhead) is detected (1) in human cell lines SH-SY5Y and MCF7, but not in mouse developing cortex or cell line NIH3T3 and (2) only upon western blotting with anti-SRGAP2 N-terminal, not with anti-SRGAP2 C-terminal.

(H) Western blotting with anti-SRGAP2 N-terminal showing knockdown of endogenous SRGAP2B or SRGAP2C, but not ancestral SRGAP2A, by siRNA against intron 9 (si-intron9-1 and -2; lane 2 and 3) in SH-SY5Y cells. See also Figure S1 and Table S1.

hESC-derived neurons (5 wic; Kim et al., 2011; lane 3 in Figure 1C). Both transcripts were also detected using RT-PCR from unpooled mRNA isolated from an individual human fetal brain (GW16; lane 4 in Figure 1C) and from the brain of a 44-year-old adult human (lane 5 in Figure 1C). In order to compare the relative level of expression of transcripts encoded by the paralogs and to tease apart transcripts derived from *SRGAP2B* and *SRGAP2C*, we took advantage of a fixed single base pair variation in exon 6 of *SRGAP2C* to design a set of primers specifically amplifying *SRGAP2C* transcripts (but not chimpanzee or human *SRGAP2A* transcripts or human *SRGAP2B* transcripts; Table S1 and Figure 1D). Quantitative-RT-PCR (qRT-PCR) revealed that both *SRGAP2C* and *SRGAP2A* transcripts were abundant in hESC-derived neurons that were cultured for 3 and 5 weeks, compared to undifferentiated hESCs (Figure 1E). However, *SRGAP2C* transcript maintained a higher level of expression than *SRGAP2A* after 5 wic (Figure 1E). This suggests that *SRGAP2C* and *SRGAP2A* transcripts do not systematically covary and might be under different regulatory mechanisms, leading to different transcript abundance in human neurons.

We next wanted to determine whether a protein product corresponding to the translation of *SRGAP2B* or *SRGAP2C* transcripts could be detected in human cells. In transfected HEK293T cells, which do not express endogenous SRGAP2, SRGAP2A could be detected in a western blot using an antibody directed against either the C-terminal (aa873-890) or the N-terminal (aa193-205) domain of the protein (Figure 1F, gray arrow). As predicted, SRGAP2C was detected as a single band of a lower molecular weight only by using the antibody directed against the N-terminal of SRGAP2 (Figure 1F, red arrow). In the human SH-SY5Y neuroblastoma cell line and the human MCF7 breast cancer cell line, a 120 kDa protein corresponding to SRGAP2A (Figure 1G, grey arrow) and a 50 kDa protein (red arrow) were detected with the N-terminal SRGAP2 antibody. The 50 kDa product was not detected in the same lysates by using the C-terminal SRGAP2 antibody, in lysates isolated from postnatal day (P) 7 mouse cortex, or from the mouse fibroblast NIH3T3 cell line, suggesting that it originates from human-specific *SRGAP2B* or *SRGAP2C* (Figure 1G). We confirmed that the 50 kDa protein product detected with the N-terminal SRGAP2 antibody in neuroblastoma SH-SY5Y cells was specifically translated from *SRGAP2B* or *SRGAP2C* by using two independent small interfering RNAs (siRNAs; called siRNA intron9-1 and intron9-2) targeting intron 9, i.e., the 3′ UTR of the endogenous *SRGAP2B* and *SRGAP2C* mRNA that is absent in endogenous *SRGAP2A* mRNA (lanes 2 and 3 in Figure 1H). The 50 kDa protein product was detected in human SH-SY5Y cells transfected with control scramble siRNA, but not in cells transfected with siRNA intron9-1 or intron9-2 (Figure 1H). Overall, our results demonstrate that *SRGAP2A* and its human-specific paralog *SRGAP2C* are expressed in fetal and adult human brains and neurons.

SRGAP2C Interacts with and Inhibits Ancestral SRGAP2 In Vitro

Next, we explored the potential function of the human-specific paralogs of *SRGAP2*. Because the F-BAR domain is a homodimerization domain involved in membrane deformation (Frost et al., 2009), and because *SRGAP2C* encodes most of the F-BAR domain of the ancestral SRGAP2A protein, we tested whether it retained the ability to dimerize with full-length SRGAP2. In HEK293T cells, hemagglutinin (HA)-tagged SRGAP2C was coexpressed with either SRGAP2A-GFP or SRGAP2C-enhanced green fluorescent protein (EGFP), followed by HA immunoprecipitation. Our results showed that SRGAP2C protein can dimerize with both SRGAP2A and SRGAP2C (Figure 2A). This suggests that the few aa substitutions in the sequence of SRGAP2C, as well as the deletion of the last 49 aa, do not alter the ability of SRGAP2C to dimerize with full-length SRGAP2A. In order to explore the biological function of SRGAP2C protein, we employed a robust membrane deformation assay in COS7 cells (Guerrier et al., 2009). As previously shown for mouse SRGAP2 (Guerrier et al., 2009), expression of human SRGAP2A-EGFP induced filopodia protrusions in COS7 cells (Figures 2B, 2C, and 2L). In contrast, expression of SRGAP2C-monomeric red fluorescent protein (mRFP) failed to induce filopodia (Figures 2D and 2L). Furthermore, when coexpressed with ancestral SRGAP2A-EGFP, SRGAP2C-mRFP efficiently blocked its ability to induce filopodia (Figures 2E and 2L). Expressing a cDNA encoding SRGAP2B (clone provided by Megan Dennis from E. Eichler's laboratory) gave similar results (Figures 2F, 2G, and 2L). Two features of SRGAP2C might account for this ability to block SRGAP2A function: (1) the mutation of several arginine residues that could mediate membrane binding/deformation properties (Shimada et al., 2007) and (2) the truncation of the F-BAR domain by deleting the last 49 aa (see Figure 1A). To test the relative contribution of these two duplicate-specific differences, we introduced these mutations individually into the native F-BAR domain of ancestral SRGAP2 (F-BAR-Δ5R and F-BAR-Δ49, respectively). Although both mutations abolished the filopodia induction properties of the F-BAR domain (Figures 2H, 2J, and 2L), only F-BAR-Δ49 mimicked SRGAP2C with regard to its ability to antagonize SRGAP2-mediated membrane protrusions (Figures 2K and 2L). Combined with the observation that the deletion of the most C-terminal 49 aa, but not the 5R mutations, is a common feature of SRGAP2C and SRGAP2B, our data suggest that both human-specific paralogs can interact with ancestral SRGAP2A and inhibit its function.

SRGAP2C Inhibits SRGAP2 Function during Cortical Neuron Migration

We then decided to test whether the human-specific duplicates of SRGAP2 can also inhibit the documented function of SRGAP2 during cortical neuron migration (Guerrier et al., 2009). We focused on SRGAP2C for further experiments because in the human brain, *SRGAP2C* transcripts are substantially more abundant than *SRGAP2B* transcripts (see accompanying paper by Dennis et al. [2012]). We used in utero electroporation to compare the in vivo function of SRGAP2 and its human-specific paralog, SRGAP2C. Mouse cortical progenitors generating layer 2/3 pyramidal neurons were electroporated at E14.5 and analyzed at E18.5, which is when most control neurons have exited the cell cycle, engaged radial migration, and a significant portion have reached their final position in the cortical plate (CP).

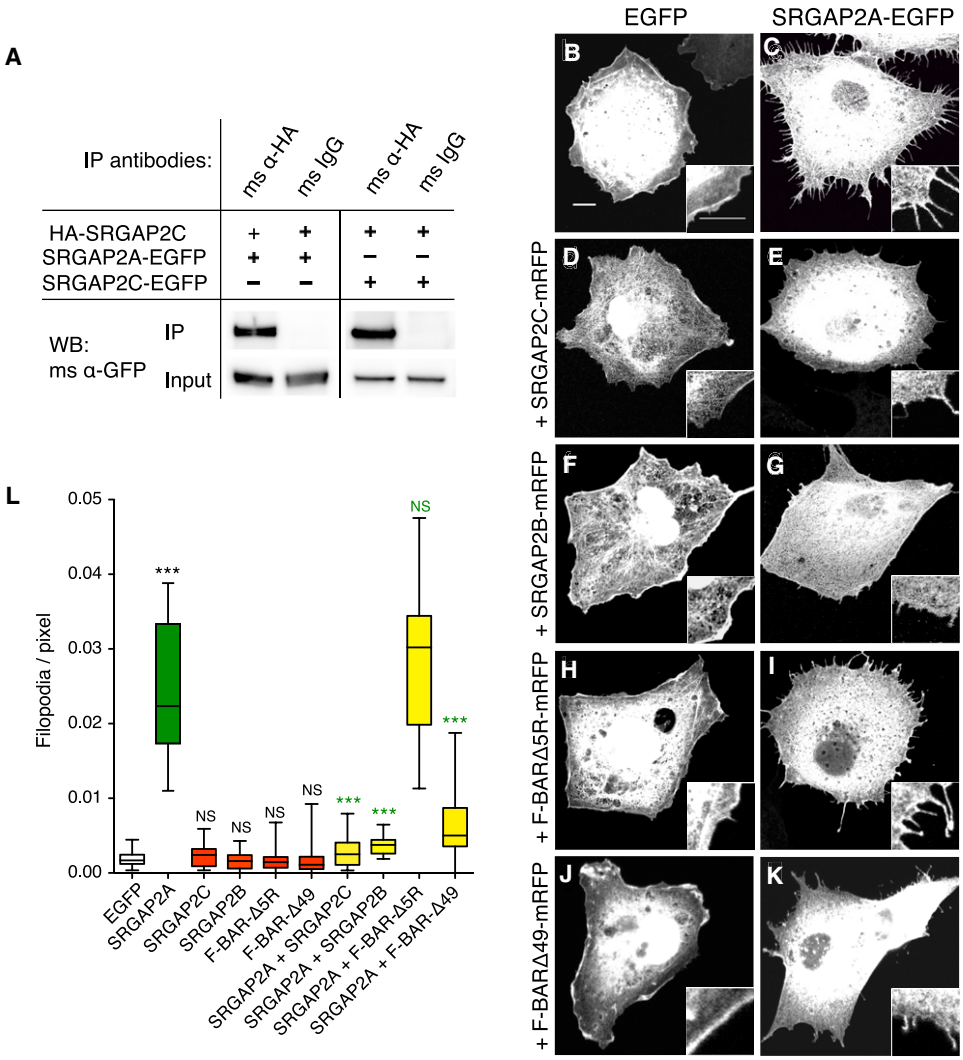

Figure 2. SRGAP2C Dimerizes with SRGAP2A and Inhibits Its Membrane Deformation Properties in COS7 Cells

(A) Coimmunoprecipitation (Co-IP) of SRGAP2A-EGFP or SRGAP2C-EGFP, along with HA-SRGAP2C in HEK293T cells, transfected with the indicated constructs. Co-IP was performed using mouse anti-HA and mouse IgG as negative control. Western blotting was performed with a mouse (ms) anti (α)-GFP.

(B–K) Representative confocal images of COS7 cells transfected with indicated constructs and visualized by EGFP signal. Scale bar, 5 μm. Inset shows 2-fold magnification.

(L) Box plot showing quantification of the number of filopodia per pixel along cell periphery for cells represented in (B–K). n = 20 cells per condition. ***$p < 0.001$, Mann-Whitney test.

As previously demonstrated for mouse SRGAP2 in ex vivo electroporated slices of embryonic cortices (Guerrier et al., 2009), overexpression of human ancestral SRGAP2A induced excessive branching of the leading process (LP) of radially migrating neurons compared to control (Figures 3A and 3B), resulting in slower migration with less neurons accumulating in the CP after 4 days in utero (Figures 3C and 3D). Conversely, knockdown of *SRGAP2* by using a short hairpin RNA (shRNA) (Figure S2) resulted in a reduction of LP branches on migrating neurons as compared to neurons expressing control shRNA (Figures 3A and 3B), and this reduction has been shown to increase the rate of migration (Guerrier et al., 2009). Interestingly, neurons expressing SRGAP2C showed a reduction in LP branching that was very similar to that seen after *SRGAP2* knockdown (Figures 3A and 3B), which results in an increased rate of radial migration as quantified by the proportion of neurons successfully reaching the CP after 4 days in utero (Figures 3C and 3D). These results support the notion that the function of ancestral SRGAP2 is conserved between mouse and human and is inhibited by SRGAP2C expression in vivo.

SRGAP2: A Postsynaptic Protein that Regulates Spine Morphology In Vitro

The expression of SRGAP2C (up to P21) in neurons generated at E15.5 did not alter the final position of neurons in layer 2/3

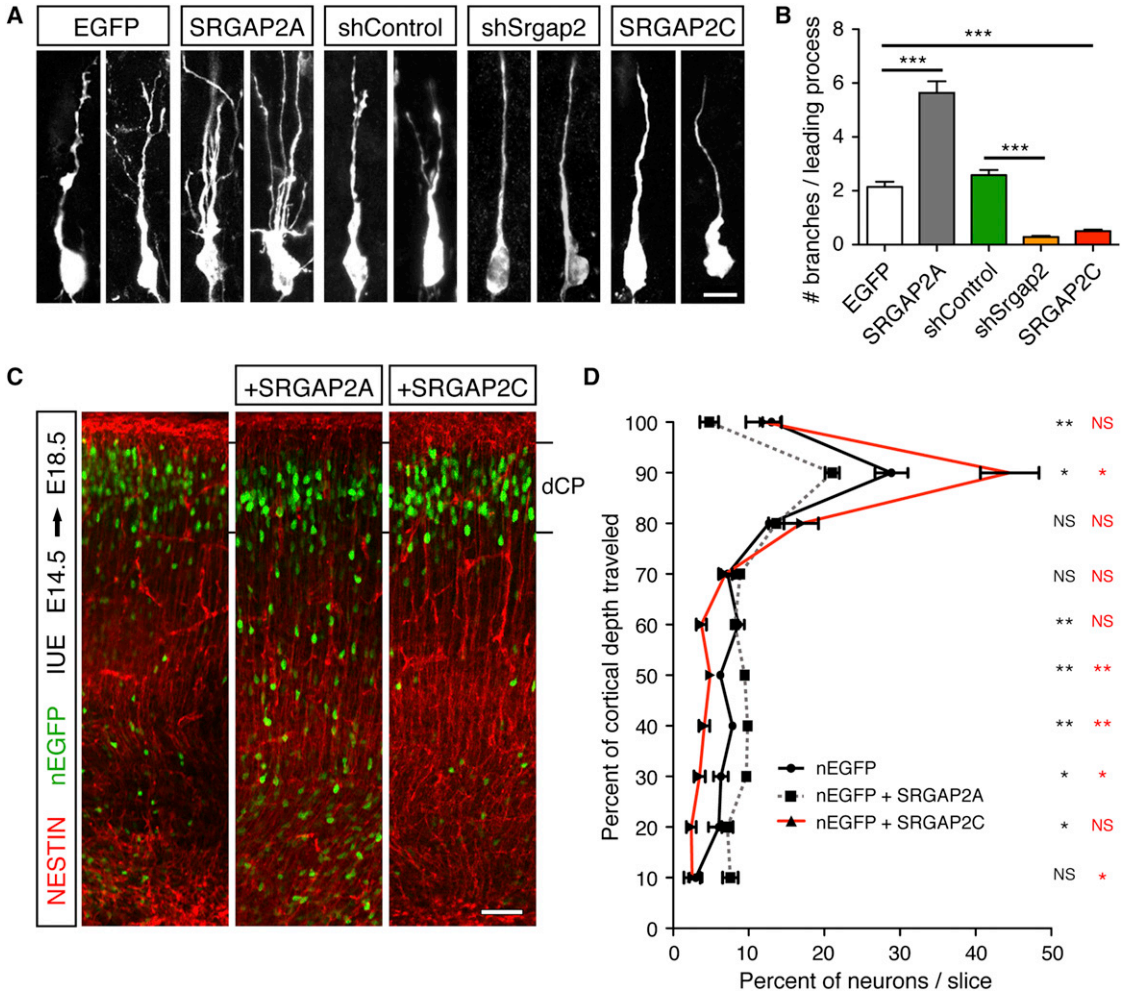

Figure 3. SRGAP2C Expression in Radially Migrating Mouse Cortical Neurons Phenocopies *Srgap2* Knockdown

(A) Confocal images of optically isolated neurons showing representative morphologies of radially migrating cortical neurons in E18.5 embryos following in utero electroporation (IUE) at E14.5 of the indicated constructs. sh, short hairpin. Scale bar, 10 μm.

(B) Mean number of branches (±SEM) of the leading process of neurons as represented in (A). n = 3 animals/condition, 100–150 neurons/condition.

(C) Low magnification confocal images of E18.5 cortical slices showing migration of in utero electroporated neurons expressing nuclear-EGFP (nEGFP) alone or together with SRGAP2A or SRGAP2C. Staining with anti-GFP shows the position of the electroporated neurons, and anti-NESTIN marks the radial glial scaffold. dCP, dense Cortical Plate.

(D) Quantification of neuron distribution in cortical slices as illustrated in (C) (mean ±SEM). n = 3 animals/condition, 9–10 slices/condition.

In (B) and (D), $*p < 0.05$; $**p < 0.01$; $***p < 0.001$; NS (not significant, $p > 0.05$); Mann-Whitney test. See also Figures S2 and S3.

compared to control (Figure S3). Indeed, although SRGAP2C expression was found to accelerate neuronal migration, this is not expected to alter cell positioning in the context of inside-out cortical neuron migration. The absence of an overt effect on neuronal placement allowed us to address the potential function of SRGAP2 at later stages of brain development. We and others have recently shown that SRGAP2 is highly expressed in the mouse neocortex during the first weeks after birth (Bacon et al., 2009; Guerrier et al., 2009), a period critical for spinogenesis and synaptogenesis in rodents (Miller, 1986; Romand et al., 2011). Therefore, we decided to investigate the currently unknown function of SRGAP2 in dendritic spines. In the neocortex, spines receive most of the excitatory connections and are a critical site of structural and functional synaptic plasticity (Holtmaat and Svoboda, 2009; Yuste and Bonhoeffer, 2001). In mouse cortical neurons cultured for 20 days in vitro (DIV), endogenous SRGAP2 showed a punctate staining that was apposed to the presynaptic marker SYNAPSIN1 and extensively colocalized with the postsynaptic marker HOMER1 (Figure 4A), indicating that SRGAP2 is enriched at excitatory synapses. Overexpression of mRFP-tagged SRGAP2 with EGFP-tagged HOMER1c showed that SRGAP2 strongly accumulates in the head of dendritic spines with HOMER1 clusters (Figure 4B). Subcellular fractionation further confirmed that SRGAP2 is associated with synaptic membranes and is detected in the postsynaptic density (Figure S4).

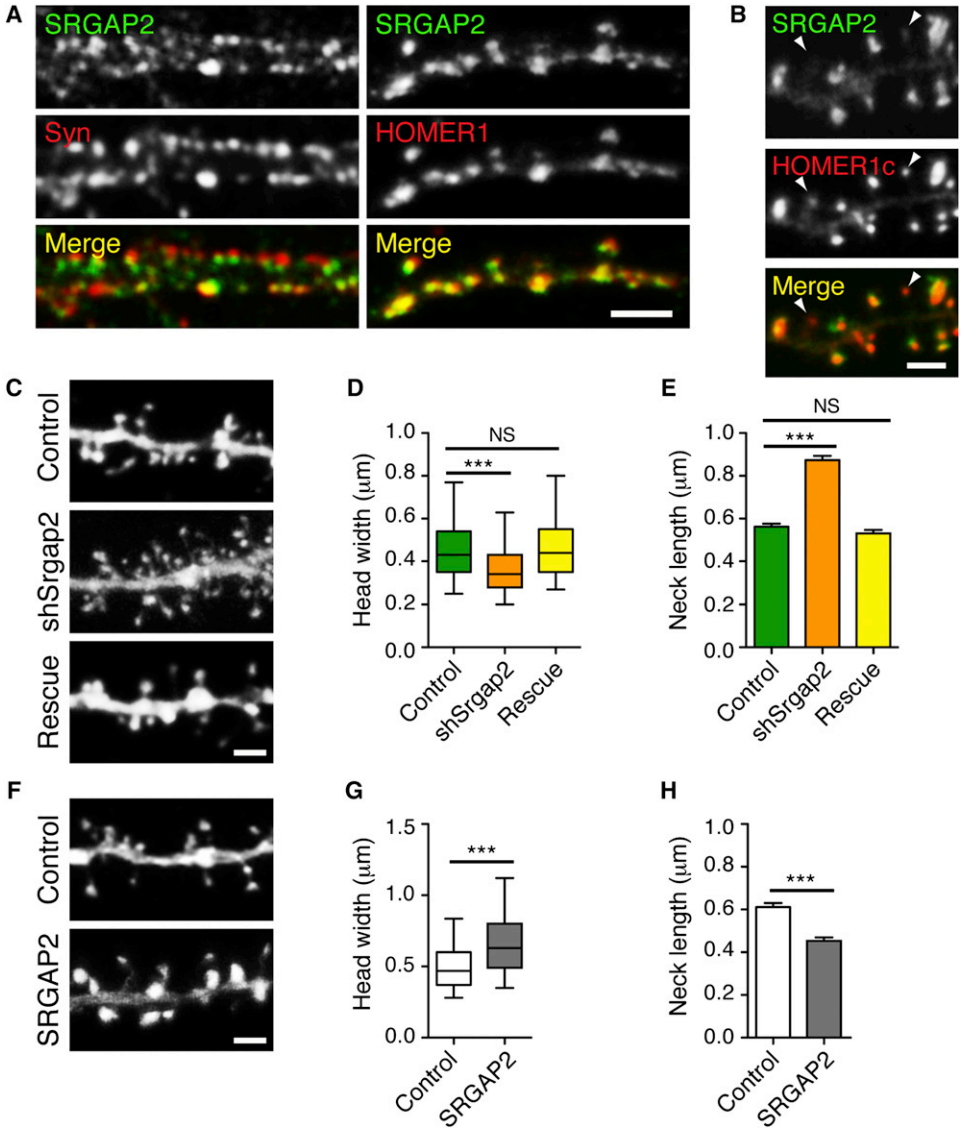

Figure 4. SRGAP2 Is Accumulated at Excitatory Synapses and Promotes Spine Head Growth in Cultured Cortical Neurons

(A) Segments of dendrites from cortical neurons (20 DIV) stained for SRGAP2 and the presynaptic marker SYNAPSIN1 (Syn) (left) or SRGAP2 and the excitatory postsynaptic marker HOMER1 (right). Scale bar, 5 μm.

(B) When overexpressed, SRGAP2-mRFP localized to the head of dendritic spines and largely colocalized with the excitatory postsynaptic marker HOMER1c-GFP. Note that SRGAP2 was barely detectable in spines with small HOMER1c clusters (arrowheads).

(C) Segments of dendrites from cortical neurons expressing a control shRNA (Control), an shRNA targeting mouse *Srgap2* (shSrgap2) and shSrgap2 coexpressed with SRGAP2A, which is resistant to this shRNA (rescue). Neurons were transfected 11 days after plating and imaged 9 days after transfection.

(D) Box plot showing the distribution of the width of spine heads in knockdown experiments. $n_{Control}$ = 1537, $n_{shSrgap2}$ = 1261, n_{rescue} = 910.

(E) Mean length of spine necks in knockdown experiments (±SEM).

(F) Segments of dendrites from cortical neurons expressing EGFP alone (control), or EGFP with ancestral SRGAP2 (SRGAP2). Neurons were transfected 17 to 18 days after plating and imaged 2 days after transfection.

(G) Distribution of the width of spine heads in gain-of-function experiments as illustrated in (F). $n_{Control}$ = 907 and n_{SRGAP2} = 1020.

(H) Mean length of spine necks in gain-of-function experiments (±SEM).

In (B), (C), and (F), scale bars, 2 μm. ***$p < 0.001$, NS: $p > 0.05$, Mann-Whitney test. Data are from a minimum of three independent experiments. See also Figures S2 and S4.

We next performed several loss- and gain-of-function experiments and measured key parameters of spine morphology: (1) the width of the spine head, which correlates with the size of the postsynaptic density, the number of synaptic AMPA glutamate receptors, and the number of presynaptic vesicles (Arellano et al., 2007; Bourne and Harris, 2007; Harris and Stevens, 1989; Matsuzaki et al., 2004) and can be used as an indicator of spine maturation (Harris and Stevens, 1989) and (2) the length

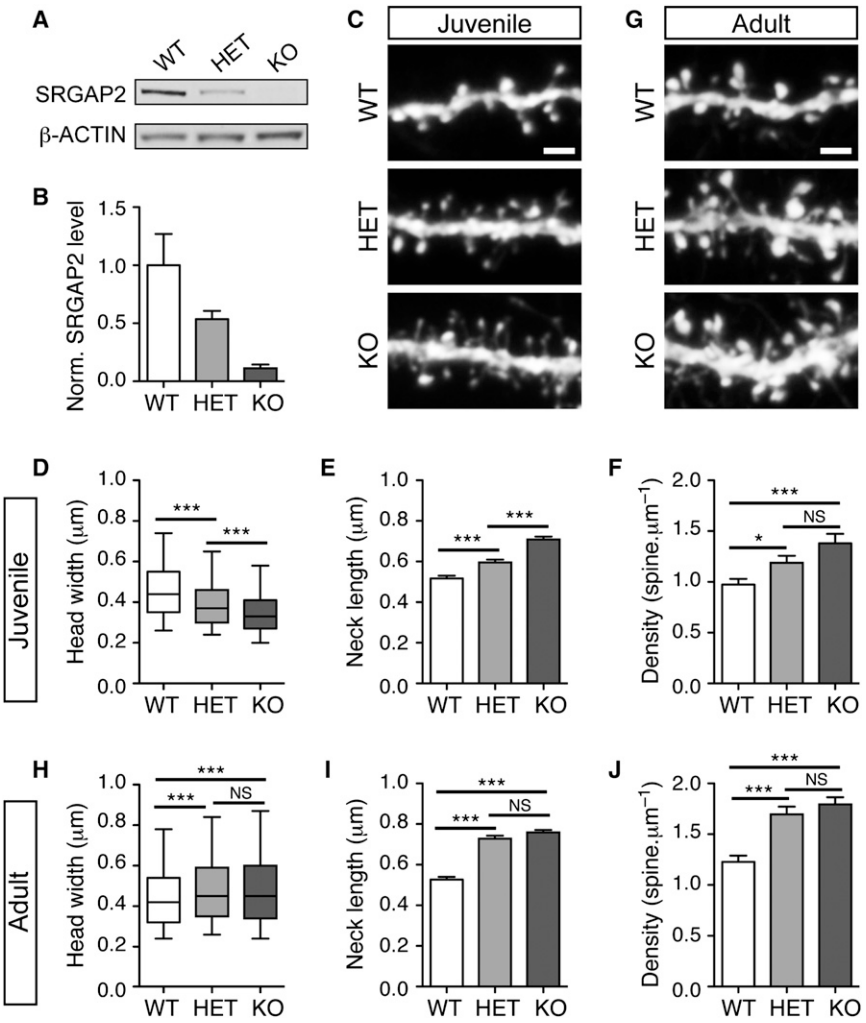

Figure 5. SRGAP2 Deficiency Delays Spine Maturation and Increases Spine Density In Vivo

(A) Representative western blot showing the relative amount of SRGAP2 in cortical lysates of wild-type (WT), heterozygous (HET), and KO mice.

(B) Quantification of SRGAP2 level in cortical lysates from three different animals per genotype normalized (norm.) to β-actin and to the average SRGAP2 level in WT.

(C–F) Dose-dependent effect of SRGAP2 deficiency in juvenile mice (P18–P21). (C) Segments of oblique dendrites from WT, HET, and KO mice expressing YFP in layer 5 pyramidal neurons (Thy1-YFP H line). (D) Distribution of spine head widths, n_{WT} = 1278, n_{HET} = 1307, and n_{KO} = 1602. (E) Mean spine neck length (±SEM). (F) Mean spine density (±SEM). n_{WT} = 26, n_{HET} = 20, and n_{KO} = 28.

(G–J) Long-term effect of SRGAP2 deficiency on dendritic spines. (G) Segments of oblique dendrites from adult (P65–P77) WT, HET, and KO mice expressing YFP in layer 5 pyramidal neurons (Thy1-YFP H line). (H) Distribution of spine head widths in adult neurons, n_{WT} = 1394, n_{HET} = 1441, and n_{KO} = 2010. (I) Mean spine neck length in adult neurons (±SEM). (J) Mean spine density (±SEM). n_{WT} = 23, n_{HET} = 23, and n_{KO} = 35. Scale bars, 2 μm. ***$p < 0.001$, NS: $p > 0.05$, Mann-Whitney test. See also Figure S5 and Table S2.

of the spine neck, which impacts the biochemical and potentially the electrical isolation of the spine head from the dendritic shaft (Araya et al., 2006; Noguchi et al., 2005; Yuste, 2011). We first studied SRGAP2 function in cultured cortical neurons by using RNA interference (see Figure S2). Plasmids expressing a control shRNA or shRNA against mouse *Srgap2* (shSrgap2) were introduced into neurons using magnetofection after 11 DIV, and spine morphology was quantified 9 to 10 days later. Neurons expressing a control shRNA (Figure 4C) exhibited spines with an average spine head width of 0.458 ± 0.004 μm (n = 1,377) (Figure 4D) and an average neck length of 0.56 ± 0.01 μm (Figure 4E). shSrgap2-expressing neurons displayed immature-looking spines (Figure 4C) with smaller head width (0.367 ± 0.004 μm, n = 1,139, Figure 4D) and longer spine neck (87 ± 0.02 μm, Figure 4E) than control shRNA-expressing neurons. We also observed an increase in spine density from 1.25 ± 0.04 spine.μm^{-1} in control neurons (n = 15) to 2.14 ± 0.13 spine.μm^{-1} in shSrgap2-expressing neurons (n = 15). The effects of SRGAP2 knockdown on spine morphology and density could be rescued by coexpressing the shRNA against *Srgap2* with an shRNA-resistant cDNA (Figures S2 and 4C–4E, density after rescue: 1.20 ± 0.06 spine.μm^{-1}, n = 15). Conversely, in gain-of-function experiments, overexpression of SRGAP2 for only 48 hr induced a striking enlargement of dendritic spines in 20 DIV neurons, as visualized by cotransfection with EGFP (Figure 4F). Upon SRGAP2 overexpression, most spines were mushroom shaped, with larger spine heads (Figure 4G) and shorter spine necks (Figure 4H) than spines in control neurons. Interestingly, SRGAP2 was barely detected in long, thin spines but was strongly accumulated in spines with large heads (see arrowheads in Figure 4B). Altogether, these results suggest that SRGAP2 is a new postsynaptic protein that promotes spine head enlargement.

SRGAP2 Promotes Spine Maturation and Limits Spine Density in the Neocortex

To obtain further insights into the function of SRGAP2 in vivo, we took advantage of a gene trap allele of *Srgap2*, hereafter called *Srgap2* KO (*SRGAP2*$^{Gt(XH102)Byg/Mmcd}$, available at MMRRC-UC Davis, Figures S5A–5C). Mapping of the insertion site in intron 2 by using an inverse PCR strategy allowed us to design a PCR genotyping protocol to distinguish the heterozygous mice from the homozygous mice (Figures S5A–5C). The homozygous *Srgap2* KO mice showed an ~90% reduction in the level of *Srgap2* transcript (Figure S5D), as well as protein (Figures 5A–5B) in the cortex, whereas heterozygous mice expressed intermediate levels of *Srgap2* mRNA and protein. *Srgap2* KO mice were viable (although born significantly below the expected

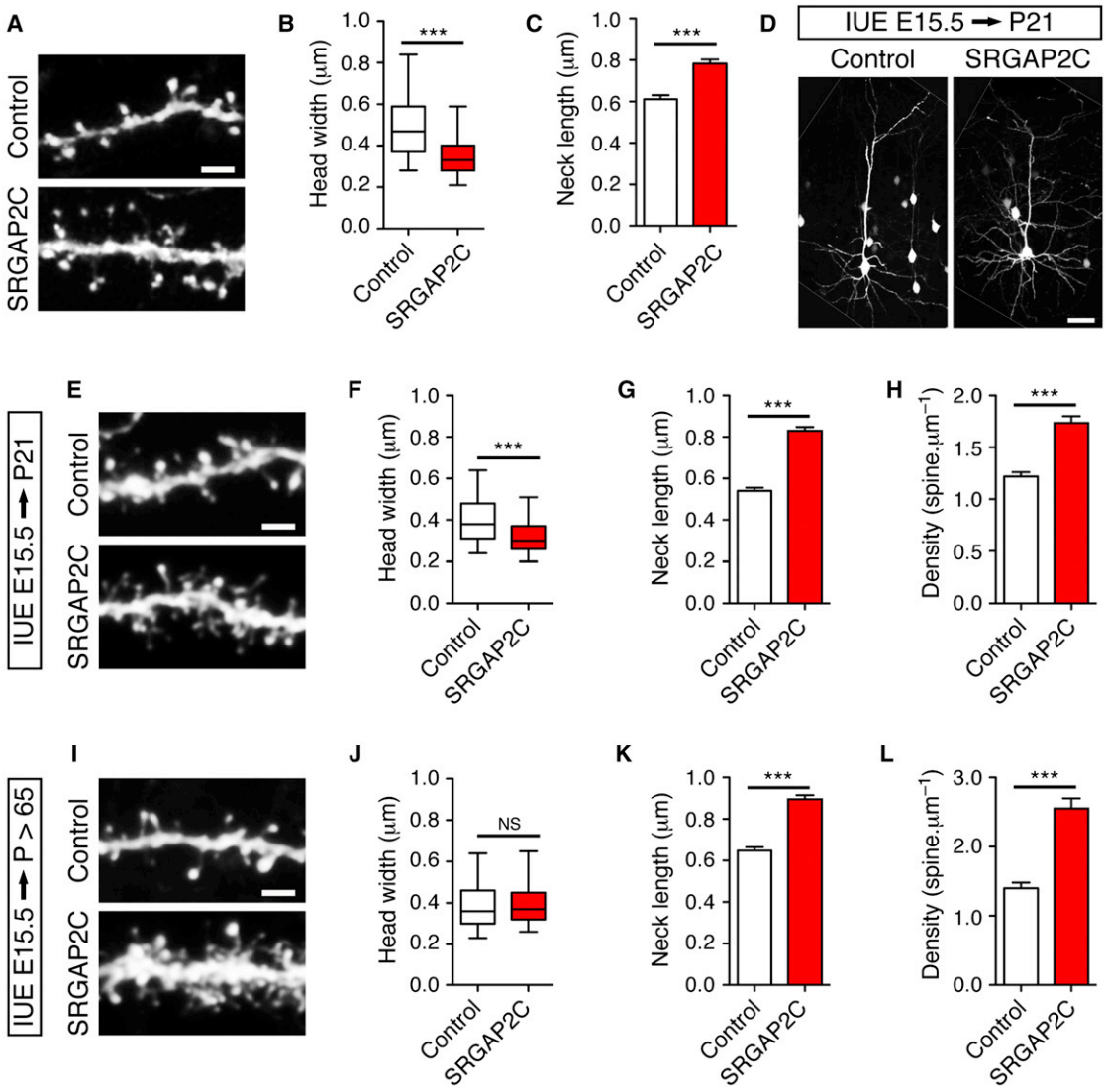

Figure 6. SRGAP2C Expression in Mouse Cortical Neurons Phenocopies SRGAP2 Deficiency in Spines

(A–C) SRGAP2C expression induces long, thin spines in cultured cortical neurons. (A) Segment of dendrites from cortical neurons (20 DIV) expressing EGFP alone (Control), or EGFP and SRGAP2C (SRGAP2C). Neurons were imaged 2 days after transfection. (B) Box plot representing the distribution of the width of spine heads. $n_{Control}$ = 907 (same as Figures 4F–4H) and $n_{SRGAP2C}$ = 1029. (C) Mean length of spine necks (±SEM).

(D–H) Effect of SRGAP2C expression in juvenile mice in layer 2/3 pyramidal neurons following in utero electroporation (IUE) at E15.5. (D) Representative layer 2/3 pyramidal neurons expressing a control cDNA (Control, left) or SRGAP2C (right) with a vector encoding mVenus. The white lines delineate the border of the original images. (E) Segments of oblique dendrites from neurons in the conditions described above. (F) Distribution of spine head widths, $n_{Control}$ = 1068, $n_{SRGAP2C}$ = 1167. (G) Mean spine neck length (±SEM). (H) Mean spine density (±SEM). $n_{Control}$ = 16 and $n_{SRGAP2C}$ = 16.

(I–L) Long-term effect of SRGAP2C expression on spines in adult mice. (I) Segments of oblique dendrites from control and SRGAP2C-expressing neurons after IUE at E15.5. (J) Distribution of spine head widths, $n_{Control}$ = 800 and $n_{SRGAP2C}$ = 941. (K) Mean spine neck length (±SEM). (L) Mean spine density (±SEM). $n_{Control}$ = 14 and $n_{SRGAP2C}$ = 12. Scale bars, 2 μm in (A), (E), and (I) and 50 μm in (D). ***$p < 0.001$, NS : $p > 0.05$, Mann-Whitney test. See also Figure S6.

Mendelian ratio; see Table S2) and showed no abnormality in cortical lamination (Figures S6A and 6B). *Srgap2* KO mice were crossed with reporter mice expressing yellow fluorescent protein (YFP) in layer 5 pyramidal neurons (Thy1-YFP line H; Feng et al., 2000), allowing quantitative assessment of dendritic spine morphology (Figure S6C). In juvenile mice (P18–P21), analysis of spines in apical oblique dendrites (see arrows in Figure S6C) of layer 5 pyramidal neurons from wild-type, heterozygous, and homozygous KO mice (Figure 5C) revealed that SRGAP2 deficiency decreased the width of spine heads (Figure 5D) and increased the length of spine necks (Figure 5E), which is consistent with the results obtained with cultured neurons. These morphological defects were associated with a marked increase in the density of dendritic spines (Figure 5F). Interestingly, these changes were dose dependent. Indeed, in juvenile mice heterozygous for *Srgap2*, spines were thinner, longer, and more numerous than in wild-type mice, but to a lesser extent than in KO mice (Figures 5C–5F).

We then wondered whether these defects were transient or maintained in adults. In adults (>P65 mice) (Figure 5G), the size of spine heads in wild-type mice was in the same range as in wild-type juveniles (Figures 5D and 5H), indicating that spines were already morphologically mature at P21. This is consistent with a previous report on the development of layer 5 pyramidal neurons (Romand et al., 2011). In contrast, heterozygous and KO neurons showed a substantial growth of their spine heads between juvenile and adult stages (Figures 5D and 5H). We observed a 22% and a 40% increase in the mean head width in heterozygous and KO neurons, respectively, so that the size of spine heads in these neurons was close to the value measured in wild-type neurons (Figure 5H) and even slightly larger (8% and 10% larger in heterozygous and KO neurons, respectively, and see Figure S6D). These data strongly suggest that SRGAP2-deficient neurons were still immature at P21 but eventually reached maturation in adults. Importantly, adult SRGAP2-deficient neurons maintained spines with longer necks and a spine density ~1.4-fold higher than in wild-type neurons (Figures 5I and 5J). Taken together, these results indicate that (1) SRGAP2 promotes spine maturation and limits spine density in vivo and (2) SRGAP2 coregulates spine density with the length of spine neck. Thus, at low SRGAP2 levels, the phase of spinogenesis is extended, and adult neurons display more numerous spines with longer necks, which may have a profound impact on neuronal connectivity and synaptic input integration.

Expression of Human-Specific SRGAP2C in Mouse Neurons Delays Spine Maturation and Increases Spine Number

Based on all the results shown so far, we hypothesized that long-term expression of the human protein SRGAP2C would delay spine maturation. In vitro, mouse cortical neurons that were maintained for 20 DIV and analyzed 2 days posttransfection of SRGAP2C displayed significant changes in spine morphology (Figures 6A–6C). These changes were opposite to the overexpression of SRGAP2 (see Figures 4F–4H) and similar to the shRNA-mediated knockdown of SRGAP2 (see Figures 4C–4E). We next analyzed in juvenile mice the consequences of SRGAP2C expression in layer 2/3 pyramidal neurons following in utero electroporation at E15.5. The coexpression of myristoylated Venus allowed the visualization of neuronal morphology (Figure 6D). As expected, in juvenile mice, SRGAP2C-expressing neurons exhibited numerous immature-looking spines as compared to control neurons (Figure 6E). Spines in SRGAP2C-expressing neurons had smaller head (Figure 6F), longer neck (Figure 6G), and were present at a higher density (Figure 6H) than in control neurons. In adult SRGAP2C-expressing neurons (Figure 6I), spine head widths were similar to control neurons (Figure 6J), but both spine neck length (Figure 6K) and spine density (Figure 6L) remained significantly higher than in control neurons. Again, these effects were highly similar to what we observed in SRGAP2-deficient layer 5 pyramidal neurons in vivo (Figures 5C–5J). Overall, these results show that expression of SRGAP2C in the mouse neocortex leads to changes in spine development that are compatible with an inhibition of endogenous SRGAP2 and result in neoteny during dendritic spine maturation.

DISCUSSION

Inhibition of SRGAP2 Function Leads to Sustained Radial Migration

Our study is among the first to address the functional consequence of human-specific gene duplication during brain development. We show that the human-specific paralogs of *SRGAP2*, along with the ancestral copy, are expressed in developing and adult neurons at the RNA and protein levels. The *SRGAP2* duplicates encode a truncated F-BAR domain that binds to and antagonizes the function of ancestral SRGAP2 during neuronal migration and morphogenesis. We previously showed that, in the mouse fetal brain, SRGAP2 is upregulated at the end of cortical migration, at which point it promotes branching in the leading process and decreases the rate of migration (Guerrier et al., 2009). Here, we found that introduction of human-specific SRGAP2C in utero in mouse pyramidal neurons mimics SRGAP2 deficiency during neuronal migration, leading to a deficit in branching in the leading process of migrating neurons and allowing neurons to reach their final position in the cortical plate faster than control neurons. We propose that these effects of human-specific SRGAP2C expression may underlie a more persistent form of radial migration and delay its termination. This could support the journey of neurons over the total thickness of the cortical wall, which is substantially increased in humans as compared to nonhuman primates or rodents (Dehay and Kennedy, 2007; Rakic, 2009; Sidman and Rakic, 1973).

Temporal Control of Spine Development

Numerous proteins have been implicated in the formation, maturation, and maintenance of spines (Bourne and Harris, 2008; Dillon and Goda, 2005; Elias et al., 2008; Hayashi et al., 2009), but the mechanisms regulating the timing of spine development in vivo remain poorly understood. In this study, we demonstrate that SRGAP2 associates with the postsynaptic density to promote spine maturation and limits spine density in vivo. In contrast, SRGAP2 deficiency or expression of SRGAP2C delays spine maturation and leads to an increased density of spines with longer necks in the neocortex. These results suggest that SRGAP2C-induced neoteny extends the period of spine production with long-term consequences on their morphology. This altered developmental trajectory of spine maturation may reflect changes in excitatory synaptic development. Other genes have been shown to produce heterochrony during organ development with critical consequences for limb morphogenesis (Dollé et al., 1993) or for the expansion of the neocortical surface (Lui et al., 2011; Rakic, 2009), supporting the notion that slower developmental processes might underlie increasingly complex morphogenesis.

Studies that have quantitatively compared spine morphology, spine density, and the developmental time course of spinogenesis between human and monkey or mouse have revealed that (1) spinogenesis in prefrontal areas presents neoteny in humans (Huttenlocher and Dabholkar, 1997; Petanjek et al., 2011); (2) spine density in comparable neocortical areas and layers is higher in humans (Benavides-Piccione et al., 2002; Elston

et al., 2001); and (3) there are substantial differences in spine morphology between species, as human spines have longer necks and larger heads than in the other species analyzed (Benavides-Piccione et al., 2002). Our results suggest that the human-specific duplication of *SRGAP2* is involved in the emergence of these differences. In the human brain, the rate of spine development differs between cortical areas (Huttenlocher and Dabholkar, 1997). Further investigations will test whether expression of SRGAP2C shows spatial heterogeneity.

Functional Implications of Human-Specific *SRGAP2* Duplication

Spines are known to enhance synaptic connectivity, enable linear integration of synaptic inputs, and implement synapse-specific plasticity (Yuste, 2011). The spine neck represents a physical barrier between the synaptic contact in the spine head and the dendritic shaft. The length of the neck impacts the compartmentalization of synaptic signaling and the filtering of synaptic inputs, whereas the volume of the spine head is an indicator of the size of the postsynaptic density and the strength of the synapse (Bourne and Harris, 2008; Yuste, 2011). Both the neck and the head of spines undergo morphological and functional plasticity (Bloodgood and Sabatini, 2005; Matsuzaki et al., 2004; Yuste and Bonhoeffer, 2001), and spines with a larger head and a wider, shorter neck have been observed after induction of synaptic potentiation in rodents (Yuste and Bonhoeffer, 2001). We found that SRGAP2 coregulates the density of spines and the length of the spine neck. Accordingly, SRGAP2-deficient neurons or SRGAP2C-expressing neurons harbored spines with longer necks and higher spine density. In our experiments, spine heads in adult SRGAP2-deficient neurons were comparable in size to wild-type neurons. In this context, we speculate that expression of SRGAP2C might allow human cortical pyramidal neurons to receive and integrate a significantly higher number of synaptic inputs without saturation. Such morphological features have been proposed to introduce more opportunities and more flexibility for input integration and information processing in human cortical circuits (Benavides-Piccione et al., 2002). On the other hand, expression of SRGAP2 might also contribute to the higher susceptibility to neurodegenerative or psychiatric disorders of the human brain (Konopka et al., 2009).

Taken together, our results suggest that the expression of SRGAP2C in the human brain inhibits the function of ancestral SRGAP2 and thereby reduces the rate of spine maturation, leading to changes in spine morphology and density that could have important implications for cognition, learning, and memory. SRGAP2 is both a membrane-binding protein and a Rho-GAP for the small GTPase Rac1, which has been associated with neurodevelopmental disorders (Govek et al., 2005). It will be important to address the molecular mechanisms by which SRGAP2 promotes spine maturation and to address how SRGAP2C interferes with this process. A large genomic alteration affecting the human ancestral *SRGAP2A* gene has recently been reported in a patient with early-infantile encephalopathy with associated epilepsy (Saitsu et al., 2011). However, this study was based on a single patient presenting a large chromosomal translocation that affected the expression of *SRGAP2A*, as well as other genes. Future investigations will test whether alterations in copy number or sequence variation of ancestral *SRGAP2A* or its human-specific paralogs underlie neurodevelopmental or cognitive defects, such as autism spectrum disorders or schizophrenia.

EXPERIMENTAL PROCEDURES

Constructs

Human *SRGAP2A* (GenBank BC132874) and *SRGAP2C* (GenBank BC112927) cDNA were obtained from the IMAGE consortium. cDNA encoding SRGAP2B was a gift from the Eichler laboratory. See Extended Experimental Procedures for details of constructs used in this paper.

RNA In Situ Hybridization

The human fetal material (GW11) used to perform in situ hybridization was collected and used according to the guidelines of the three relevant local ethics committees on research involving human subjects (Erasme Academic Hospital, University of Brussels, and Belgian National Fund for Scientific Research). Written informed consent was given by the parents in each case. Exon 22 of *SRGAP2A* (3316-4271 base pairs [bp] of BC132874) and intron 9 (1992-3128 bp of BC112927) were amplified and cloned into pGEM-T Easy Vector System 1 (Promega), and they served as templates for generating RNA in situ probes. In situ hybridization on human embryonic brain samples was performed as previously described (Lambert et al., 2011).

Animals

All animals were handled according to protocols approved by the institutional animal care and use committee (IACUC) at the University of North Carolina at Chapel Hill and The Scripps Research Institute, La Jolla. For timed pregnant matings, noon after mating is considered embryonic day 0.5 (E0.5). Juveniles correspond to mice between postnatal day (P) 18 and P21, and adults correspond to mice between P65 and P77. For information regarding genetic strains, refer to Extended Experimental Procedures.

In Utero Electroporation

We performed in utero electroporation as per a previously described protocol (Yi et al., 2010). Endotoxin-free plasmid DNA was injected at a concentration of 1 μg/μl in the lateral ventricles. In case of coelectroporation, we injected equimolar quantities of the two plasmids to ensure coexpression. Please see Extended Experimental Procedures for electroporation settings, tissue preparation, slicing, and immunostaining of electroporated brains.

Primary Neuronal Culture, Magnetofection, and Immunocytochemistry

Primary cultures of cortical neurons were prepared from embryonic BALB/c mice at days 17.5–18.5 and transfection was performed by magnetofection using NeuroMag (OZ Bioscience) according to the manufacturer's protocol at the indicated times. See details in Extended Experimental Procedures.

Morphometric Analysis of Spines

Morphometric analyses of dendritic spines were performed on z-projections for cultured neurons and in the depth of the z stack for slices using NIS-Elements (Nikon imaging software). Head width was defined as the largest length of the head that was perpendicular to the neck. Neck length was measured from the point of attachment of the dendrite to the beginning of the spine head, as estimated by the investigator. When the neck could not be distinguished from the head, the neck length was considered to be zero. When the neck was not clearly visible, it was considered to be the shortest distance between the base of the head and the closest surface of the dendrite. Only spines arising from the lateral surfaces of the dendrites were taken into account. For analyses in slices, spines were quantified in the proximal part of oblique dendrites directly originating from the apical trunk. Spines were quantified over an average of 60 μm of dendrite in juvenile mice and 40 μm in adult mice. Spine density was defined as the number of quantified spines divided by the length over which the spines were quantified. The length of

the dendritic segment was measured on the z projection, which implies that the density could be overestimated. To limit this issue, only dendrites that were parallel to the plane of the slice were analyzed. Spine analysis in vivo was analyzed in brain sections of comparable rostro-caudal position. See Extended Experimental Procedures for more details.

Subcellular Fractionation

Subcellular fractionation was performed from P15 mouse brains as described in Pérez-Otaño et al. (2006) with minor modifications. See Extended Experimental Procedures for details of antibodies used.

SUPPLEMENTAL INFORMATION

Supplemental Information includes Extended Experimental Procedures, six figures, and two tables and can be found with this article online at doi:10.1016/j.cell.2012.03.034.

ACKNOWLEDGEMENTS

We would like to thank Marie Rougié and Virginie Courchet for excellent technical support and management of the mouse colonies and members of the Polleux laboratory for useful discussions. We thank Maxime Camo for help with the initial characterization of the SRGAP2 KO, Daniel Choquet for providing HOMER1c expression plasmid, and Evan Eichler's lab for reagents and useful discussions. N.L. is a clinical scientist of the FNRS and P.V. is a Research Director of the FNRS. This work was partially supported by grants of the FNRS, Belgian Queen Elizabeth Foundation, Welbio and Excellence Programs of the Walloon Region (to P.V.), Fonds Erasme and the Belgian Kids' Fund (to N.L.), NIH RO1NS067557 (F.P.) and ADI-Novartis funds (F.P.), NIH F31NS061610 (J.d.M.), NIH F31NS068038 (J.C.-B.), by NSFC (No.31171033), and "973" Project (No.2011CB933101) (W.-L.J.). C.C., K.J., T.S. and F.P. conceived the experiments, and C.C., K.J., J.C.-B., J.d.M., T.S., N.L., and P.V. performed the experiments. W.-L.J. provided the anti-SRGAP2 antibodies. J.-E.K. and A.G. provided RNA from cultured human ES cells. C.C., K.J., and F.P. prepared the manuscript. A.G. is currently an employee of F. Hoffmann La Roche.

Received: December 12, 2011
Revised: February 28, 2012
Accepted: March 1, 2012
Published online: May 3, 2012

REFERENCES

Araya, R., Jiang, J., Eisenthal, K.B., and Yuste, R. (2006). The spine neck filters membrane potentials. Proc. Natl. Acad. Sci. USA *103*, 17961–17966.

Arellano, J.I., Benavides-Piccione, R., Defelipe, J., and Yuste, R. (2007). Ultrastructure of dendritic spines: correlation between synaptic and spine morphologies. Front Neurosci. *1*, 131–143.

Bacon, C., Endris, V., and Rappold, G. (2009). Dynamic expression of the Slit-Robo GTPase activating protein genes during development of the murine nervous system. J. Comp. Neurol. *513*, 224–236.

Bailey, J.A., and Eichler, E.E. (2006). Primate segmental duplications: crucibles of evolution, diversity and disease. Nat. Rev. Genet. *7*, 552–564.

Bailey, J.A., Gu, Z., Clark, R.A., Reinert, K., Samonte, R.V., Schwartz, S., Adams, M.D., Myers, E.W., Li, P.W., and Eichler, E.E. (2002). Recent segmental duplications in the human genome. Science *297*, 1003–1007.

Benavides-Piccione, R., Ballesteros-Yáñez, I., DeFelipe, J., and Yuste, R. (2002). Cortical area and species differences in dendritic spine morphology. J. Neurocytol. *31*, 337–346.

Bloodgood, B.L., and Sabatini, B.L. (2005). Neuronal activity regulates diffusion across the neck of dendritic spines. Science *310*, 866–869.

Bourne, J., and Harris, K.M. (2007). Do thin spines learn to be mushroom spines that remember? Curr. Opin. Neurobiol. *17*, 381–386.

Bourne, J.N., and Harris, K.M. (2008). Balancing structure and function at hippocampal dendritic spines. Annu. Rev. Neurosci. *31*, 47–67.

Calarco, J.A., Xing, Y., Cáceres, M., Calarco, J.P., Xiao, X., Pan, Q., Lee, C., Preuss, T.M., and Blencowe, B.J. (2007). Global analysis of alternative splicing differences between humans and chimpanzees. Genes Dev. *21*, 2963–2975.

Dehay, C., and Kennedy, H. (2007). Cell-cycle control and cortical development. Nat. Rev. Neurosci. *8*, 438–450.

Dennis, M.Y., Nuttle, X., Sudmant, P.H., Antonacci, F., Graves, T.A., Nefedov, M., Rosenfeld, J.A., Sajjadian, S., Malig, M., Kotkiewicz, H., et al. (2012). Evolution of human-specific neural SRGAP2 genes by incomplete segmental duplication. Cell *149*. Published online May 3, 2012. 10.1016/j.cell.2012.03.033.

Dillon, C., and Goda, Y. (2005). The actin cytoskeleton: integrating form and function at the synapse. Annu. Rev. Neurosci. *28*, 25–55.

Dollé, P., Dierich, A., LeMeur, M., Schimmang, T., Schuhbaur, B., Chambon, P., and Duboule, D. (1993). Disruption of the Hoxd-13 gene induces localized heterochrony leading to mice with neotenic limbs. Cell *75*, 431–441.

Elias, G.M., Elias, L.A., Apostolides, P.F., Kriegstein, A.R., and Nicoll, R.A. (2008). Differential trafficking of AMPA and NMDA receptors by SAP102 and PSD-95 underlies synapse development. Proc. Natl. Acad. Sci. USA *105*, 20953–20958.

Elston, G.N., Benavides-Piccione, R., and DeFelipe, J. (2001). The pyramidal cell in cognition: a comparative study in human and monkey. J. Neurosci. *21*, RC163.

Enard, W., Przeworski, M., Fisher, S.E., Lai, C.S., Wiebe, V., Kitano, T., Monaco, A.P., and Pääbo, S. (2002). Molecular evolution of FOXP2, a gene involved in speech and language. Nature *418*, 869–872.

Feng, G., Mellor, R.H., Bernstein, M., Keller-Peck, C., Nguyen, Q.T., Wallace, M., Nerbonne, J.M., Lichtman, J.W., and Sanes, J.R. (2000). Imaging neuronal subsets in transgenic mice expressing multiple spectral variants of GFP. Neuron *28*, 41–51.

Fortna, A., Kim, Y., MacLaren, E., Marshall, K., Hahn, G., Meltesen, L., Brenton, M., Hink, R., Burgers, S., Hernandez-Boussard, T., et al. (2004). Lineage-specific gene duplication and loss in human and great ape evolution. PLoS Biol. *2*, E207.

Frost, A., Unger, V.M., and De Camilli, P. (2009). The BAR domain superfamily: membrane-molding macromolecules. Cell *137*, 191–196.

Govek, E.E., Newey, S.E., and Van Aelst, L. (2005). The role of the Rho GTPases in neuronal development. Genes Dev. *19*, 1–49.

Guerrier, S., Coutinho-Budd, J., Sassa, T., Gresset, A., Jordan, N.V., Chen, K., Jin, W.L., Frost, A., and Polleux, F. (2009). The F-BAR domain of srGAP2 induces membrane protrusions required for neuronal migration and morphogenesis. Cell *138*, 990–1004.

Harris, K.M., and Stevens, J.K. (1989). Dendritic spines of CA 1 pyramidal cells in the rat hippocampus: serial electron microscopy with reference to their biophysical characteristics. J. Neurosci. *9*, 2982–2997.

Hayashi, M.K., Tang, C., Verpelli, C., Narayanan, R., Stearns, M.H., Xu, R.M., Li, H., Sala, C., and Hayashi, Y. (2009). The postsynaptic density proteins Homer and Shank form a polymeric network structure. Cell *137*, 159–171.

Holtmaat, A., and Svoboda, K. (2009). Experience-dependent structural synaptic plasticity in the mammalian brain. Nat. Rev. Neurosci. *10*, 647–658.

Hurles, M. (2004). Gene duplication: the genomic trade in spare parts. PLoS Biol. *2*, E206.

Huttenlocher, P.R., and Dabholkar, A.S. (1997). Regional differences in synaptogenesis in human cerebral cortex. J. Comp. Neurol. *387*, 167–178.

Itoh, T., Erdmann, K.S., Roux, A., Habermann, B., Werner, H., and De Camilli, P. (2005). Dynamin and the actin cytoskeleton cooperatively regulate plasma membrane invagination by BAR and F-BAR proteins. Dev. Cell *9*, 791–804.

Kim, J.E., O'Sullivan, M.L., Sanchez, C.A., Hwang, M., Israel, M.A., Brennand, K., Deerinck, T.J., Goldstein, L.S., Gage, F.H., Ellisman, M.H., and Ghosh, A. (2011). Investigating synapse formation and function using human pluripotent stem cell-derived neurons. Proc. Natl. Acad. Sci. USA *108*, 3005–3010.

Konopka, G., Bomar, J.M., Winden, K., Coppola, G., Jonsson, Z.O., Gao, F., Peng, S., Preuss, T.M., Wohlschlegel, J.A., and Geschwind, D.H. (2009). Human-specific transcriptional regulation of CNS development genes by FOXP2. Nature *462*, 213–217.

Lambert, N., Lambot, M.A., Bilheu, A., Albert, V., Englert, Y., Libert, F., Noel, J.C., Sotiriou, C., Holloway, A.K., Pollard, K.S., et al. (2011). Genes expressed in specific areas of the human fetal cerebral cortex display distinct patterns of evolution. PLoS ONE *6*, e17753.

Lui, J.H., Hansen, D.V., and Kriegstein, A.R. (2011). Development and evolution of the human neocortex. Cell *146*, 18–36.

Matsuzaki, M., Honkura, N., Ellis-Davies, G.C., and Kasai, H. (2004). Structural basis of long-term potentiation in single dendritic spines. Nature *429*, 761–766.

McLean, C.Y., Reno, P.L., Pollen, A.A., Bassan, A.I., Capellini, T.D., Guenther, C., Indjeian, V.B., Lim, X., Menke, D.B., Schaar, B.T., et al. (2011). Human-specific loss of regulatory DNA and the evolution of human-specific traits. Nature *471*, 216–219.

Miller, M.W. (1986). Maturation of rat visual cortex. III. Postnatal morphogenesis and synaptogenesis of local circuit neurons. Brain Res. *390*, 271–285.

Noguchi, J., Matsuzaki, M., Ellis-Davies, G.C., and Kasai, H. (2005). Spine-neck geometry determines NMDA receptor-dependent Ca2+ signaling in dendrites. Neuron *46*, 609–622.

Ohno, S. (1970). Evolution by Gene Duplication (New York: Springer-Verlag).

Pérez-Otaño, I., Luján, R., Tavalin, S.J., Plomann, M., Modregger, J., Liu, X.B., Jones, E.G., Heinemann, S.F., Lo, D.C., and Ehlers, M.D. (2006). Endocytosis and synaptic removal of NR3A-containing NMDA receptors by PACSIN1/syndapin1. Nat. Neurosci. *9*, 611–621.

Petanjek, Z., Judaš, M., Šimic, G., Rasin, M.R., Uylings, H.B., Rakic, P., and Kostovic, I. (2011). Extraordinary neoteny of synaptic spines in the human prefrontal cortex. Proc. Natl. Acad. Sci. USA *108*, 13281–13286.

Pollard, K.S., Salama, S.R., Lambert, N., Lambot, M.A., Coppens, S., Pedersen, J.S., Katzman, S., King, B., Onodera, C., Siepel, A., et al. (2006). An RNA gene expressed during cortical development evolved rapidly in humans. Nature *443*, 167–172.

Prabhakar, S., Noonan, J.P., Pääbo, S., and Rubin, E.M. (2006). Accelerated evolution of conserved noncoding sequences in humans. Science *314*, 786.

Prabhakar, S., Visel, A., Akiyama, J.A., Shoukry, M., Lewis, K.D., Holt, A., Plajzer-Frick, I., Morrison, H., Fitzpatrick, D.R., Afzal, V., et al. (2008). Human-specific gain of function in a developmental enhancer. Science *321*, 1346–1350.

Rakic, P. (2009). Evolution of the neocortex: a perspective from developmental biology. Nat. Rev. Neurosci. *10*, 724–735.

Romand, S., Wang, Y., Toledo-Rodriguez, M., and Markram, H. (2011). Morphological development of thick-tufted layer V pyramidal cells in the rat somatosensory cortex. Front. Neuroanat. *5*, 5.

Saitsu, H., Osaka, H., Sugiyama, S., Kurosawa, K., Mizuguchi, T., Nishiyama, K., Nishimura, A., Tsurusaki, Y., Doi, H., Miyake, N., et al. (2011). Early infantile epileptic encephalopathy associated with the disrupted gene encoding Slit-Robo Rho GTPase activating protein 2 (SRGAP2). Am. J. Med. Genet. A. *158A*, 199–205.

Shimada, A., Niwa, H., Tsujita, K., Suetsugu, S., Nitta, K., Hanawa-Suetsugu, K., Akasaka, R., Nishino, Y., Toyama, M., Chen, L., et al. (2007). Curved EFC/F-BAR-domain dimers are joined end to end into a filament for membrane invagination in endocytosis. Cell *129*, 761–772.

Sidman, R.L., and Rakic, P. (1973). Neuronal migration, with special reference to developing human brain: a review. Brain Res. *62*, 1–35.

Sikela, J.M. (2006). The jewels of our genome: the search for the genomic changes underlying the evolutionarily unique capacities of the human brain. PLoS Genet. *2*, e80.

Stankiewicz, P., and Lupski, J.R. (2010). Structural variation in the human genome and its role in disease. Annu. Rev. Med. *61*, 437–455.

Sudmant, P.H., Kitzman, J.O., Antonacci, F., Alkan, C., Malig, M., Tsalenko, A., Sampas, N., Bruhn, L., Shendure, J., and Eichler, E.E.; 1000 Genomes Project. (2010). Diversity of human copy number variation and multicopy genes. Science *330*, 641–646.

Varki, A., Geschwind, D.H., and Eichler, E.E. (2008). Explaining human uniqueness: genome interactions with environment, behaviour and culture. Nat. Rev. Genet. *9*, 749–763.

Yi, J.J., Barnes, A.P., Hand, R., Polleux, F., and Ehlers, M.D. (2010). TGF-beta signaling specifies axons during brain development. Cell *142*, 144–157.

Yuste, R. (2011). Dendritic spines and distributed circuits. Neuron *71*, 772–781.

Yuste, R., and Bonhoeffer, T. (2001). Morphological changes in dendritic spines associated with long-term synaptic plasticity. Annu. Rev. Neurosci. *24*, 1071–1089.

EXTENDED EXPERIMENTAL PROCEDURES

Cell Line Culture and Filopodia Assay

COS7 (CRL-1651), HEK293T (CRL-1573), SH-SY5Y (CRL-2266), MCF7 (HTB-22) and HeLa (CCL-2) cell lines were obtained from ATCC and cultured according to suggested protocols. Unless indicated otherwise, transfection of cell lines was performed using Jet-Prime (Polyplus Transfection). To test filopodia induction, COS7 cells were transfected with the indicated constructs, trypsinized at 12 hours post-transfection and replated onto Poly-D-Lysine (PDL)-coated coverslips for an additional 12 hours. The cells were fixed using 4% paraformaldehyde and mounted using Vectashield (Vector labs). Cell imaging and quantification is detailed below.

Cell Lysis, Coimmunoprecipitation

Cultured cells or brain tissue were collected and lysed by homogenizing in RIPA buffer (1% NP-40, 0.5% sodium deoxycholate, 0.1% sodium dodecyl sulphate, 150 mM sodium chloride in 50 mM Tris buffer at pH 8). For co-immunoprecipitation, 1 mg of total protein from each sample was incubated overnight with Protein A-agarose beads (Roche) and either 1 μg of mouse anti-HA antibody (*HA.11* Clone 16B12 Monoclonal Antibody, Covance) or 1 μg of mouse IgG as negative control. The beads were collected by centrifugation and washed in RIPA lysis buffer with 250 mM sodium chloride. Finally, the beads were resuspended in gel-loading buffer and bound proteins were released with boiling.

Western Blotting

Samples were loaded on a Mini-Protean TGX (4-15%) SDS-PAGE gel (BIORAD). Western blotting was performed using mouse anti-GFP (Invitrogen, 1:1000), mouse anti-actin (Invitrogen, 1:5000), rabbit-anti-SRGAP2 C-terminal (raised against residues 873-890, 1:2000; [Guerrier et al., 2009]), rabbit-anti-SRGAP2 N-terminal (raised against residues 193-205, 1:2000; Abgent), mouse anti-SAP102 (Neuromab; 1:2000), mouse anti-synaptophysin1 (Synaptic Systems,1:5000) antibodies and HRP-conjugated secondary antibodies. They were revealed by chemiluminescence.

Constructs

The human *SRGAP2A* cDNA from BC132874 was cloned into pEGFP-N1 with C-terminal fusion to EGFP. The *SRGAP2A*-EGFP cassette was then subcloned into pCIG2 (Hand et al., 2005) by replacing the IRES-GFP fragment. The resulting clone had a CMV-enhancer/chicken-β-actin promoter driving the expression of a SRGAP2A-EGFP fusion protein. The human SRGAP2A protein is 98% identical to the previously characterized mouse SRGAP2 protein. *SRGAP2B* and *SRGAP2C* were cloned similarly. From these constructs, mRFP-tagged or HA-tagged versions were derived by replacing EGFP with PCR amplified mRFP, or multimerized (3X) HA tag, respectively. F-BAR-Δ49 (aa 1-452) was cloned using PCR amplification from *SRGAP2A*-EGFP. F-BAR-Δ5R was cloned by swapping the region containing the 5 R mutations in BC112927 into the F-BAR domain of SRGAP2A (aa 1-501). For tracking migrating neurons, we replaced the IRES-EGFP cassette in pCIG2 with EGFP-NLS (nuclear localization signal). The Homer1c-EGFP construct (Bats et al., 2007) was a kind gift from Daniel Choquet (Université Bordeaux 2, France).

siRNA, shRNA Constructs and Validation

We modified pSilencer2.1 (Invitrogen) to co-express myristoylated-Venus (mVenus) driven by the CAG promoter in addition to the U6-driven shRNA and named this vector pSCV2 (pSilencer2.1-CAG-Venus) (Hand and Polleux, 2011). We then replaced the U6 promoter with H1 promoter and named this vector pH1-SCV2. The control scrambled shRNA seed sequence was 5′-ACA CCT ATA ACA ACG GTA G-3′. shRNA against mouse *Srgap2* used the seed sequence 5′-CTA TCT GCT GAA TTA AAT C-3′. To validate this shRNA, we co-expressed it with mouse *Srgap2*-EGFP (Guerrier et al., 2009) or human *SRGAP2A*-EGFP at a 2:1 ratio in HeLa cells. Three days after transfection, cells were lysed in RIPA buffer (see above). The relative expression levels of SRGAP2 and shRNA vector were detected by western blotting using a mouse anti-GFP antibody (1:2000, Invitrogen) (see Figure S2). The shRNA was highly efficient to knock-down mouse Srgap2-EGFP expression. Human SRGAP2A was insensitive to the shRNA and was used in rescue experiments. For knocking down SRGAP2B and SRGAP2C, we purchased from EUROFIN, siRNA duplexes against two target sequences in the 3′ UTR of *SRGAP2B* and *SRGAP2C*: Intron9-1 (5′-ACA CCT AAA GGT GCA AAC ATT AA-3′) and Intron9-2 (5′-AAG GAC AGG CAT TGA ATA TCT TA-3′). For control siRNA, we used Accell Red Non-Targeting siRNA (Dharmacon). In order to validate the siRNA-mediated knock-down, we transfected SH-SY5Y cells using Lipofectamine2000 (Invitrogen). A transfection efficiency of >90% was estimated using fluorescent signal from the control siRNA. Efficiency of the knock-down was tested by western blotting using the anti-SRGAP2 N-terminal antibody (see Figure 1H).

RT-PCR

For in vitro differentiation of hESCs, total RNA was received from the laboratory of Dr. Anirvan Ghosh (Kim et al., 2011). The following mRNA from human brain samples was purchased from BioChain: Fetal mRNA, GW16 (M1244142) and Adult mRNA, 44 years old (M1234122). Adult chimp brain RNA was a kind gift from Dr. Evan Eichler (Univ. Washington, Seattle). cDNA synthesis was performed from 1 μg RNA using SuperScript III (Invitrogen) and primed with oligodT primers. RT-PCR was performed using Taq DNA polymerase (New England Biolabs). Quantitative-RT-PCR (Q-RT-PCR) was performed using the RotorGene RG-3000 thermocycler (Corbett

Research) and GoTaq qPCR mastermix (Promega). The primers used and the sizes of amplification products are indicated in Table S1.

Mouse Strains

The Thy1-YFP H strain was B6.Cg-Tg(Thy1-YFPH)2Jrs/J (Feng et al., 2000), obtained from Jackson Laboratory. Genotyping was performed according to Jackson Laboratory recommendation. The *Srgap2* knock-out strain was a gene trapped (GT) allele of *Srgap2* (*B6;129P2-Srgap2*$^{Gt(XH102)Byg/Mmcd}$) obtained from Mutant Mouse Regional Resource Centers (MMRRC). Mice homozygous for this allele were referred to as *Srgap2* KO (knock-out). Inverse PCR was performed to identify the integration site of the gene trap vector pGT1Lxf (Ochman et al., 1988). Tail genomic DNA from wild-type, heterozygous and KO mice was digested with NcoI or EcoRI, ligated using T4 DNA ligase (New England Biolabs) and used as a template for PCR using the following primers that bind to the gene trap vector: NcoI forward 5′-AGC ACG TAC TCG GAT GGA AG-3′; NcoI reverse 5′-CCG TAA TGG GAT AGG TTA CG-3′; EcoRI forward 5′-CAG CAA CTG ATG GAA ACC AG-3′; and EcoRI reverse 5′-ACC GGC TAA AAC TTG AGA CC-3′. A single fragment was amplified from each reaction, and sequencing analysis identified a vector-free 134 bp sequence 5′ to the integrated gene trap vector. BLAST analysis mapped the sequence to intron 2 of mouse *Srgap2* with 98.5% (132/134) identity. Mice were genotyped after ethanol precipitation of genomic DNA from tail lysate. The PCR reactions used the following primers: primer A (forward) 5′-CTC TCA GGA CTT TAC TCT GC-3′, primer B (WT reverse) 5′-CAA AGA TAG AGC TGC AAC CAC-3′ and primer C (GT reverse) 5′-ACC GGC TAA AAC TTG AGA CC-3′. The wild-type allele was detected using primer A and primer B as a 512 bp fragment, while the gene trapped allele was detected using primer A and primer C as a 396 bp fragment (see Figure S5).

In Utero Electroporation

The previously described protocol for in utero electroporation (Yi et al., 2010) was modified as follows. Two sets of electroporation settings were used: (i) For experiments involving short-term prenatal effects, we used timed pregnant C57BL/6 females and performed in utero electroporation at E14.5 followed by short-term survival until E18.5. The electroporation settings were as follows: 4 pulses of 40 V for 50 ms with 500 ms interval. (ii) For in utero electroporation combined with survival after birth, we used timed pregnant F1 females from C57BL/6 X 129/SvJ (The Jackson Laboratory). Electroporation was performed at E15.5 to target cortical layer 2/3. The electroporation settings were: 4 pulses of 45 V for 50 ms with 500 ms interval.

Tissue Preparation, Slicing, and Immunostaining

Animals at the indicated age were anaesthetized with isofluorane before intracardiac perfusion with PBS and 4% PFA (Electron Microscopy Sciences). 100 μm coronal brain sections were obtained using a vibrating microtome (Leica VT1200S). Sections were mounted in Vectashield or, when indicated, processed for immunostaining. Briefly, the immunostaining protocol involved overnight incubation of the slices in primary antibodies diluted in blocking solution (0.1% Triton-X100, 5% goat serum, 1% BSA in PBS), followed by three washes in PBS and incubation in secondary antibodies (Invitrogen) diluted in blocking solution. Excess secondary antibody was removed by washing three times in PBS and slices were mounted on slides using Vectashield mounting medium.

Primary Neuronal Culture, Magnetofection, and Immunocytochemistry

Cortices from E17.5-18.5 were dissected in Hank's Buffered Salt Solution (HBSS) supplemented with Hepes (10 mM) and glucose (0.66 M, Sigma). Cortices were dissociated in papain (Worthington) supplemented with DNAse I (100 μg/ml, Sigma) for 20 min at 37°C, washed three times and manually triturated in plating medium supplemented with DNAse. Cells were then plated at 5.5 x 10^4 cells per cm^2 on glass bottom dishes coated with poly-D-lysine (1 mg/ml, Sigma) and cultured for 5 days in neurobasal medium supplemented with 2.5% fetal bovine serum (Gemini), B27 (1X), L-glutamine (2 mM) and penicillin (2.5 units/ml)-streptomycin (2.5 μg/ml). Unless otherwise indicated, all products were from Invitrogen. After 5 days in vitro, half of the medium was replaced with serum-free medium and one third of the medium was then changed every 5 days. After 10 days in vitro, 5-Fluoro-5′-deoxyuridine (Sigma) was added to the culture medium at a final concentration of 5 μM to limit glia proliferation. Cells were maintained at 37°C in 5% CO2 for 20 days. To transfect cultured neurons, we performed magnetofection using NeuroMag (OZ Bioscience) according to the manufacturer's protocol. Cotransfections were performed at a 1:1 ratio (w/w). For knock-down experiments, the shRNA vector was expressed alone, with pCIG2 or with SRGAP2A (rescue experiments). Because no difference in spine morphology was observed after transfection of the shRNA vector alone and the shRNA vector with pCIG2 (data not shown), data were pooled together. For immunocytochemistry, cells were fixed for 15 min at room temperature in 4% (w/v) paraformaldehyde in PBS, and incubated for 30 min in 0.1% Triton X100, 1% BSA (Sigma) in PBS to permeabilize and block nonspecific staining. Primary and secondary antibodies were diluted in the buffer described above. Primary antibodies were incubated for 1 hour at room temperature and secondary antibodies were incubated for 45 min at room temperature. Coverslips were mounted on slides with Vectashield (Vector Laboratories).

Antibodies Used for Immunocytochemistry and Immunohistochemistry

Primary antibodies used in this study are rabbit anti-CUX1 (M-222, 0.4 μg/ml, Santa Cruz), rabbit anti-TBR1 (1:500, Abcam), mouse anti-SYNAPSIN1 (0.5 μg/ml, Synaptic System), mouse anti-HOMER1 (5 μg/ml, Synaptic System), mouse anti-NESTIN (0.5 μg/ml, BD Bioscience), chicken anti-GFP (5 μg/ml, Aves Lab) rabbit-anti-SRGAP2 C-terminal (1:200; Guerrier et al., 2009). All secondary

antibodies were Alexa-conjugated (Invitrogen) and used at a 1:1000 dilution. Nuclear DNA was stained using Hoechst 33258 (1:10000, Pierce) or Draq5 (1:10000, Alexis).

Image Acquisition and Analyses

Images were acquired in 1024x1024 mode with a Nikon Ti-E microscope equipped with the A1 laser scanning confocal microscope using the Nikon software NIS-Elements (Nikon Corporation, Melville, NY). We used the following objective lenses (Nikon): 10x PlanApo; NA 0.45 (for images of cortical slices and migration analyses), 60x Apo TIRF; NA 1.49 (for images of COS-7, analyses of branching in the leading process and morphometric analyses of spines in cultured neurons), 100X H-TIRF; NA 1.49 (for images of spines in slices). To quantify the number of filopodia per cell, ImageJ was used to trace a line outside the cell periphery such that it cut across the filopodia. The number of filopodia was counted and plotted as a ratio of the length of the line. Quantification of neuron migration and branching in the leading process of migrating neurons were performed as previously described (Guerrier et al., 2009).

Statistics

Statistical analyses were performed with Prism (GraphPad Software). Chi-square test was used to determine whether the observed distribution of *Srgap2* KO animals at birth follows the expected Mendelian distribution. For other sets of data, we first checked the normality of the distributions using the one-sample Kolmogorov-Smirnov test and non-normal distributions were assessed using the Mann-Whitney test. A test was considered significant when $p < 0.05$. Unless otherwise noted data are expressed as mean ±SEM. For dendritic spine analysis, all data were obtained from at least three independent experiments or at least three animals. For morphometric analyses of spines in slices, we decided to compare the distributions of the data after pooling. However, data were consistent between litters and between animals and similar results were obtained when spine head widths or neck lengths were averaged by dendrite before statistical comparison.

SUPPLEMENTAL REFERENCES

Bats, C., Groc, L., and Choquet, D. (2007). The interaction between Stargazin and PSD-95 regulates AMPA receptor surface trafficking. Neuron *53*, 719–734.

Feng, G., Mellor, R.H., Bernstein, M., Keller-Peck, C., Nguyen, Q.T., Wallace, M., Nerbonne, J.M., Lichtman, J.W., and Sanes, J.R. (2000). Imaging neuronal subsets in transgenic mice expressing multiple spectral variants of GFP. Neuron *28*, 41–51.

Guerrier, S., Coutinho-Budd, J., Sassa, T., Gresset, A., Jordan, N.V., Chen, K., Jin, W.L., Frost, A., and Polleux, F. (2009). The F-BAR domain of srGAP2 induces membrane protrusions required for neuronal migration and morphogenesis. Cell *138*, 990–1004.

Hand, R., and Polleux, F. (2011). Neurogenin2 regulates the initial axon guidance of cortical pyramidal neurons projecting medially to the corpus callosum. Neural Develop. *6*, 30.

Hand, R., Bortone, D., Mattar, P., Nguyen, L., Heng, J.I., Guerrier, S., Boutt, E., Peters, E., Barnes, A.P., Parras, C., et al. (2005). Phosphorylation of Neurogenin2 specifies the migration properties and the dendritic morphology of pyramidal neurons in the neocortex. Neuron *48*, 45–62.

Kim, J.E., O'Sullivan, M.L., Sanchez, C.A., Hwang, M., Israel, M.A., Brennand, K., Deerinck, T.J., Goldstein, L.S., Gage, F.H., Ellisman, M.H., and Ghosh, A. (2011). Investigating synapse formation and function using human pluripotent stem cell-derived neurons. Proc. Natl. Acad. Sci. USA *108*, 3005–3010.

Ochman, H., Gerber, A.S., and Hartl, D.L. (1988). Genetic applications of an inverse polymerase chain reaction. Genetics *120*, 621–623.

Yi, J.J., Barnes, A.P., Hand, R., Polleux, F., and Ehlers, M.D. (2010). TGF-beta signaling specifies axons during brain development. Cell *142*, 144–157.

A

QUERY	SCORE	START	END	QSIZE	IDENTITY	CHRO	STRAND	START	END	SPAN
BC13287	4352	331	4710	4710	100.0%	1	+	204582823	204702814	119992
BC13287	923	492	1426	4710	99.7%	1	+	120808675	120831215	22541
BC13287	545	9	558	4710	99.9%	1	+	142627521	142805783	178263

B

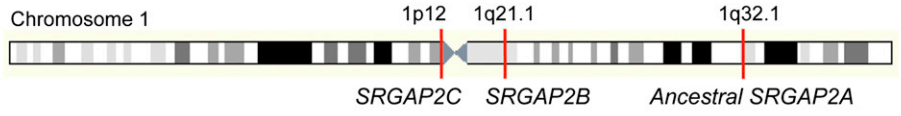

C

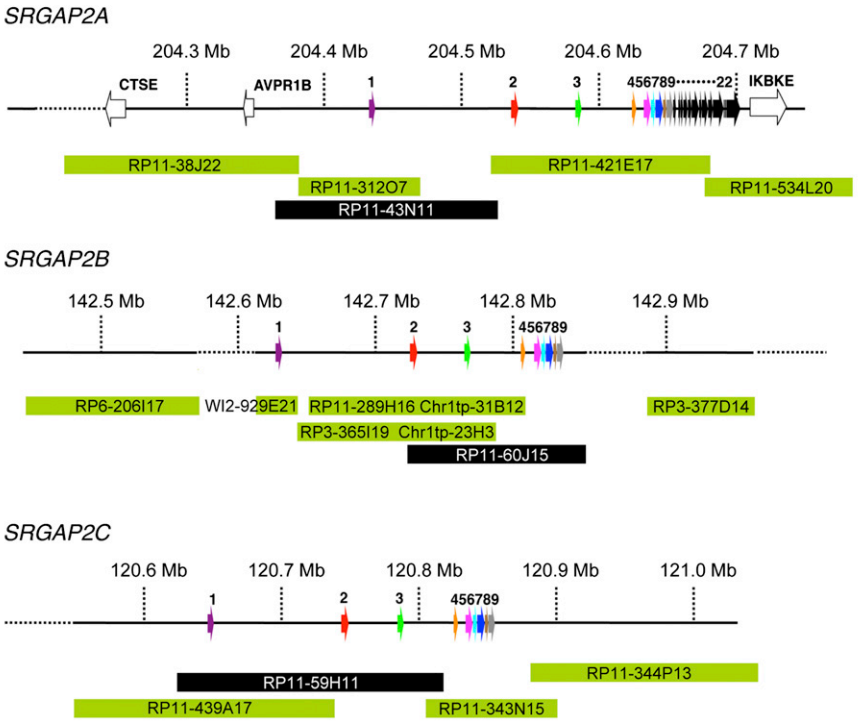

Figure S1. Identification of Human Paralogs of *SRGAP2*, Related to Figure 1

(A) Results of a BLAT search of the human genome (assembly GRCh36/hg18) using *SRGAP2* cDNA clone BC132874 as query. Only hits with identity >99% are shown. Qsize stands for query size.

(B) Schematic representation of the location of the three *SRGAP2* paralogs on chromosome1.

(C) Schematic representation of the genomic structure of the paralogs of *SRGAP2* as revealed by BAC mapping. Exons of ancestral *SRGAP2* are indicated by colored arrows. Neighboring genes are indicated by white arrows. BAC clones mapped on human reference assembly GRCh36 are depicted by green arrows. BAC clones shown in black boxes represent those identified by BLAST search against the end sequences database using flanking genome sequences as inputs.

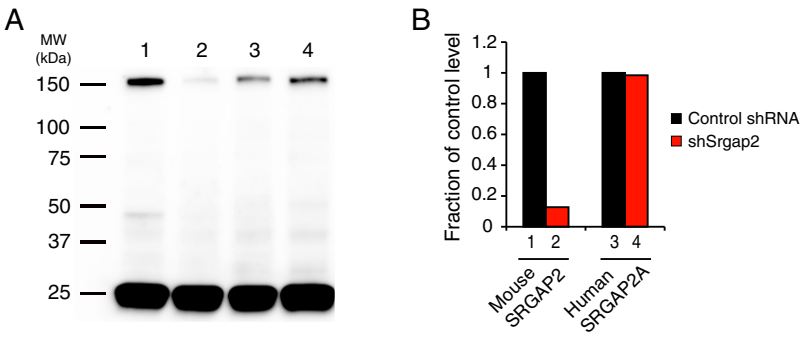

Figure S2. Validation of Mouse *Srgap2* Knockdown Using shRNA, Related to Figures 3 and 4

(A) Western blot showing the knock-down efficacy of the shRNA against mouse *Srgap2*. Hela cells were co-transfected with a control shRNA (lanes 1 and 3) or a shRNA directed against mouse *Srgap2* (lanes 2 and 4) and a cDNA encoding EGFP-tagged mouse SRGAP2 (lanes 1 and 2) or EGFP-tagged human SRGAP2A (lanes 3 and 4). There is a three base pair difference between the mouse *Srgap2* and the human *SRGAP2A* sequences in the region targeted by the shRNA. Because the shRNA vector expressed myristoylated Venus (mVenus, a membrane-bound EGFP variant) in addition to the shRNA, the levels of expression of both SRGAP2 and the shRNA vector could be visualized in western blot using a mouse anti-GFP antibody. GFP-SRGAP2 was detected as a single band migrating at 150 kDa (upper band) whereas mVenus had an apparent molecular weight (MW) of 25 kDa (lower band).

(B) Quantification of mouse (left) and human (right) SRGAP2 levels in control and knock-down (shSrgap2) conditions. SRGAP2 signal was normalized to the amount of mVenus in the same lane and expressed as a fraction of SRGAP2 level in the corresponding control condition. Chemiluminescence was quantified on non-saturated images. Note that shSrgap2 does not target human *SRGAP2A* so that the human *SRGAP2A* cDNA could be used for rescue experiments.

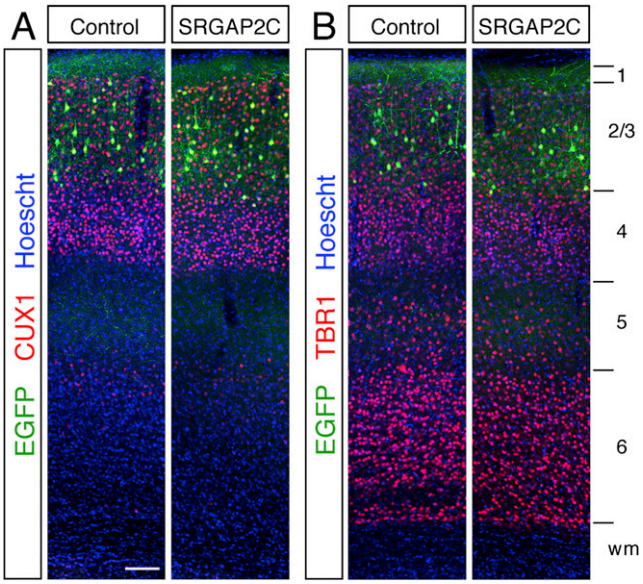

Figure S3. Absence of Neuronal Positioning Defects following Expression of SRGAP2C, Related to Figures 3 and 6

(A and B) Low magnification confocal images of P21 cortical slices showing the position of neurons electroporated in utero at E15.5 and expressing mVenus together with EGFP (control) or SRGAP2C. Sections were stained with CUX1 (red, specific for layers 2–4) (A), or TBR1 (red, specific for layers 4 and 6) (B) and the nuclear marker Hoescht for cytoarchitecture. wm: white matter. Scale bar, 100 μm.

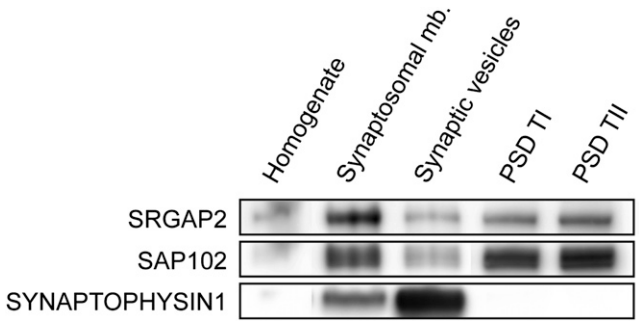

Figure S4. SRGAP2 Associates with the Postsynaptic Density, Related to Figure 4

Immunoblots of homogenates and synaptic fractions from P15 mouse brains. Mb.: membrane, PSD TI-II, progressively Triton X100-insoluble fractions of the postsynaptic density (PSD). For western blotting, 15 μg of each sample was loaded on the gel. The membrane was cut to show the fractions of interest. Note that SRGAP2 is enriched in the synaptosomal and postsynaptic fractions as observed for SAP102.

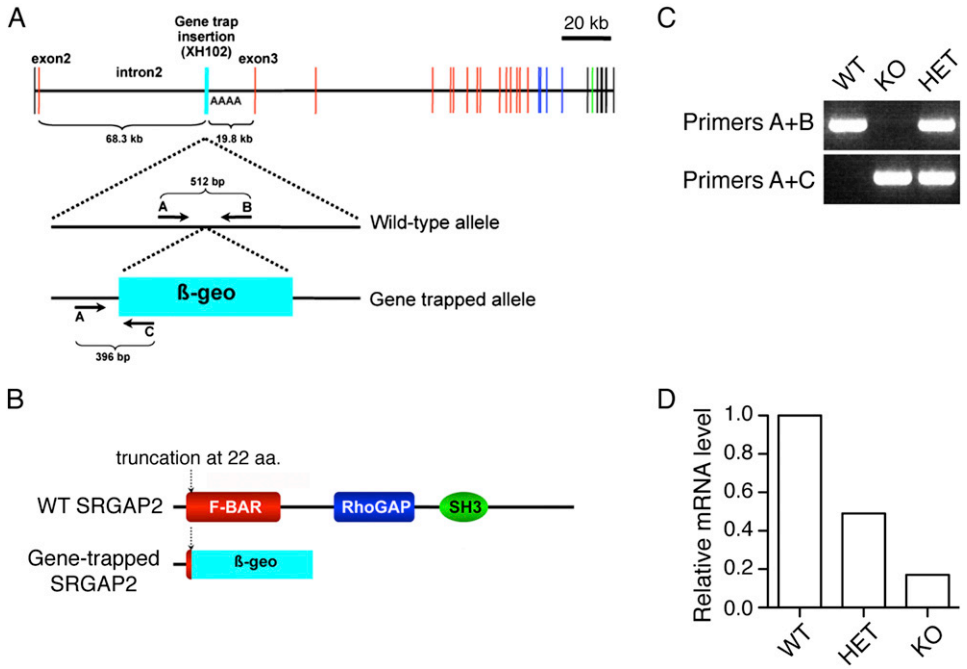

Figure S5. *Srgap2* Gene Targeting in the *SRGAP2*$^{Gt(XH102)Byg/Mmcd}$ Gene Trap Allele, Related to Figure 5

(A) Schematic representation of the genomic organization of the *Srgap2* mouse gene locus on Chromosome 1 showing the gene-trap insertion and the strategy for genotyping. Coding exons are represented in red (encoding the F-BAR domain), blue (encoding the Rho-GAP domain) and green (C-terminal domain containing the SH3 domain).

(B) The resulting gene-trap allele leads to the production of a fusion protein composed of the first 22 aa of SRGAP2 and β-Geo.

(C) Genotyping of wild-type (WT), heterozygous (HET) and KO mice with the primers shown in panel A. We refer to animals homozygous for the gene-trap allele as KO mice.

(D) qRT-PCR assay using primers recognizing the exon 2-3 junction of mouse *Srgap2* in total RNA from P7 brains. Data are normalized to β-ACTIN levels and expressed as a fraction of wild-type levels.

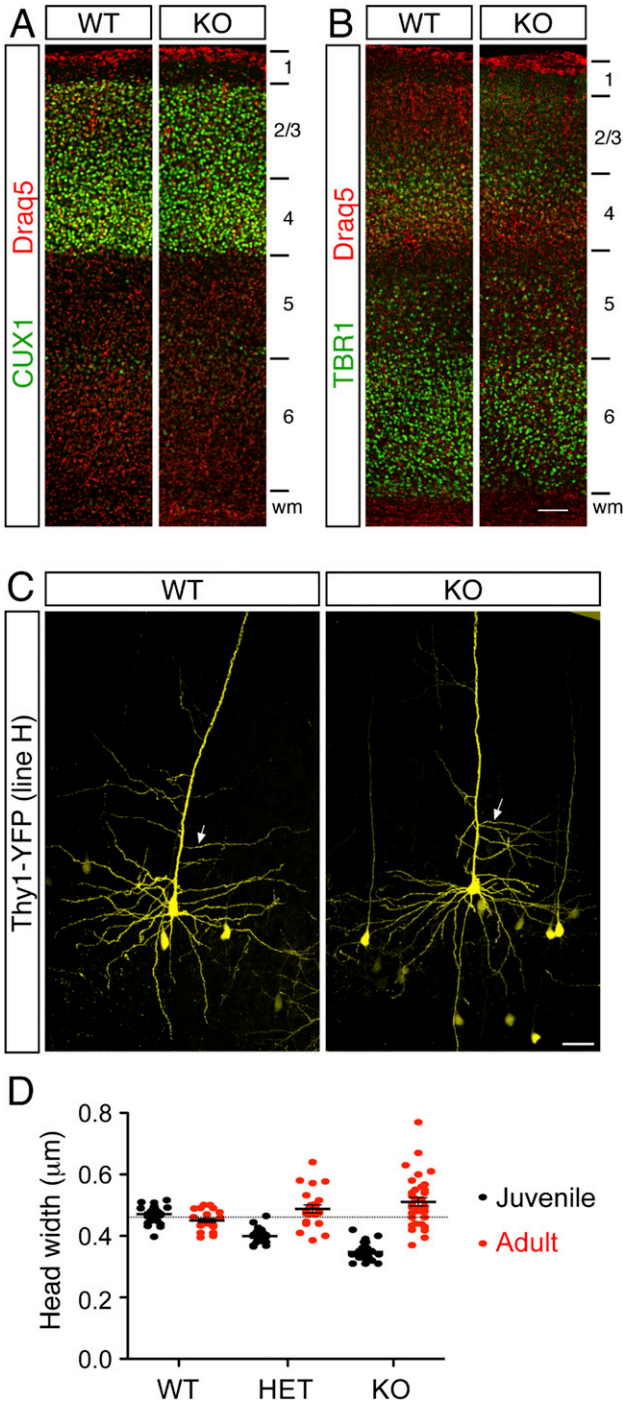

Figure S6. Absence of Migration Defects in the Cortex of *Srgap2* Knockout Mice, Related to Figure 6

(A) Expression of the layer 2–4-specific marker CUX1 (green) in cortical slices from P21 wild-type (WT, left) and *Srgap2* KO (right) mice. Sections were counterstained with the nuclear marker draq5 (red) for cytoarchitecture.

(B) Expression of the layer 4- and 6-specific marker TBR1 (green) in cortical slices from P21 wild-type (left) and *Srgap2* KO (right) mice. Sections were counterstained with the nuclear marker draq5 (red). Note that CUX1 and TBR1 staining were undistinguishable between wild-type and KO mice.

(C) *Srgap2* wild-type and KO mice were crossed with the Thy1-YFP line H reporter (Feng et al., 2000) in order to visualize the morphology of layer 5 pyramidal neurons. Arrows indicate the position of oblique dendrites emerging from the apical trunk that were used for quantitative analysis of spine morphology and density. Scale bar, 100 μm (panels A-B); 40 μm (panel C).

(D) Plot showing the distribution of the mean spine head width for all dendritic segments analyzed in juvenile (black) and adult (red) wild-type, heterozygous (HET) and KO mice. In each condition, the black lines represent the mean ±SEM. The dashed line indicates the mean head width in wild-type mice (juveniles and adults).